



Modeling of the chemistry in oxidation flow reactors with high initial NO

Zhe Peng and Jose L. Jimenez

Cooperative Institute for Research in Environmental Sciences and Department of Chemistry, University of Colorado, Boulder, CO 80309, USA

Correspondence to: Zhe Peng (zhe.peng@colorado.edu) and Jose L. Jimenez (jose.jimenez@colorado.edu)

Received: 22 March 2017 – Discussion started: 10 April 2017

Revised: 28 August 2017 – Accepted: 4 September 2017 – Published: 10 October 2017

Abstract. Oxidation flow reactors (OFRs) are increasingly employed in atmospheric chemistry research because of their high efficiency of OH radical production from low-pressure Hg lamp emissions at both 185 and 254 nm (OFR185) or 254 nm only (OFR254). OFRs have been thought to be limited to studying low-NO chemistry (in which peroxy radicals (RO_2) react preferentially with HO_2) because NO is very rapidly oxidized by the high concentrations of O_3 , HO_2 , and OH in OFRs. However, many groups are performing experiments by aging combustion exhaust with high NO levels or adding NO in the hopes of simulating high-NO chemistry (in which $\text{RO}_2 + \text{NO}$ dominates). This work systematically explores the chemistry in OFRs with high initial NO. Using box modeling, we investigate the interconversion of N-containing species and the uncertainties due to kinetic parameters. Simple initial injection of NO in OFR185 can result in more RO_2 reacted with NO than with HO_2 and minor non-tropospheric photolysis, but only under a very narrow set of conditions (high water mixing ratio, low UV intensity, low external OH reactivity (OHR_{ext}), and initial NO concentration (NO^{in}) of tens to hundreds of ppb) that account for a very small fraction of the input parameter space. These conditions are generally far away from experimental conditions of published OFR studies with high initial NO. In particular, studies of aerosol formation from vehicle emissions in OFRs often used OHR_{ext} and NO^{in} several orders of magnitude higher. Due to extremely high OHR_{ext} and NO^{in} , some studies may have resulted in substantial non-tropospheric photolysis, strong delay to RO_2 chemistry due to peroxyxynitrate formation, VOC reactions with NO_3 dominating over those with OH, and faster reactions of OH–aromatic adducts with NO_2 than those with O_2 , all of which are irrelevant to am-

bient VOC photooxidation chemistry. Some of the negative effects are the worst for alkene and aromatic precursors. To avoid undesired chemistry, vehicle emissions generally need to be diluted by a factor of > 100 before being injected into an OFR. However, sufficiently diluted vehicle emissions generally do not lead to high-NO chemistry in OFRs but are rather dominated by the low-NO $\text{RO}_2 + \text{HO}_2$ pathway. To ensure high-NO conditions without substantial atmospherically irrelevant chemistry in a more controlled fashion, new techniques are needed.

1 Introduction

The oxidation of gases that are emitted into the atmosphere, in particular volatile organic compounds (VOCs), is one of the most important atmospheric chemistry processes (Haagen-Smit, 1952; Chameides et al., 1988). VOC oxidation is closely related to radical production and consumption (Levy II, 1971), O_3 production, and the formation of secondary aerosols (Odum et al., 1996; Hoffmann et al., 1997; Volkamer et al., 2006; Hallquist et al., 2009), which have impacts on air quality and climate (Lippmann, 1991; Nel, 2005; Stocker et al., 2014).

Chemical reactors are critical tools for research of VOC oxidation. Oxidation reactions of interest often have typical timescales of hours to weeks. Studying these processes in ambient air can be confounded by dispersion and changes in ambient conditions, which often occur on similar timescales. Chemical reactors allow for the decoupling of these two types of processes. Also, they should be able to simulate the different regimes of reactions occurring in the atmosphere,

e.g., VOC oxidation under the low- and high-NO conditions (peroxy radical fate dominated by reaction with HO₂ or NO) representing remote and urban areas, respectively (Orlando and Tyndall, 2012).

Large environmental chambers are a commonly used reactor type (Carter et al., 2005; Wang et al., 2011). They typically employ actinic wavelength (> 300 nm) light sources (e.g., outdoor solar radiation and UV black lights) to produce oxidants and radicals and have large volumes (on the order of several cubic meters or larger). However, the capability of generating sustained elevated levels of OH, the most important tropospheric oxidant, is usually limited in chambers, resulting in OH concentrations similar to those in the atmosphere (10⁶–10⁷ molecules cm⁻³; Mao et al., 2009; Ng et al., 2010) and consequently long simulation times (typically hours) to reach OH equivalent ages of atmospheric relevance (George et al., 2007; Kang et al., 2007; Carlton et al., 2009; Seakins, 2010; Wang et al., 2011). The partitioning of gases and aerosols to chamber walls (usually made of Teflon) in timescales of tens of minutes to hours makes it difficult to conduct very long experiments that simulate high atmospherically relevant photochemical ages (Cocker et al., 2001; Matsunaga and Ziemann, 2010; Zhang et al., 2014; Krechmer et al., 2016). In addition, the long simulation times and large size of chambers and auxiliary equipment are logistically difficult for field deployment, and their cost limits the number of laboratories equipped with them.

Given the limitations of environmental chambers, a growing number of experimenters have instead employed oxidation flow reactors (OFRs). OFRs have a much smaller size (on the order of 10 L), efficiently generate OH via photolysis of H₂O and/or O₃ by more energetic 185 and 254 nm photons from low-pressure Hg lamps, and overcome the abovementioned shortcomings of chambers due to a much shorter residence time (George et al., 2007; Kang et al., 2007, 2011; Lambe et al., 2011). Moreover, OFRs are able to rapidly explore a wide range of OH equivalent ages within a short period (~2 h) during which significant changes in ambient conditions can usually be avoided in the case of field deployment (Ortega et al., 2016; Palm et al., 2016, 2017). Because of these advantages, OFRs have recently been widely used to study atmospheric chemistry, in particular secondary organic aerosol (SOA) formation and aging, in both the laboratory and the field (Kang et al., 2011; Li et al., 2013; Ortega et al., 2013, 2016; Tkacik et al., 2014; Palm et al., 2016).

In addition to experimental studies using OFRs, there has also been some progress in the characterization of OFR chemistry by modeling. Li et al. (2015) and Peng et al. (2015) developed a box model for OFR HO_x chemistry that predicts measurable quantities (e.g., OH exposure, OH_{exp}, in molecules cm⁻³ s and O₃ concentration, abbr. O₃ hereinafter, in ppm) in good agreement with experiments. This model has been used to characterize HO_x chemistry as a function of H₂O mixing ratio (abbr. H₂O hereinafter, unitless), UV light intensity (abbr. UV hereinafter, in photons cm⁻² s⁻¹),

and external OH reactivity (in s⁻¹, OHR_{ext} = ∑ k_i c_i, i.e., the sum of the products of concentrations of externally introduced OH-consuming species, c_i, and rate constants of their reactions with OH, k_i). Based on this characterization, Peng et al. (2015) found that OH suppression, i.e., the reduction of OH concentration caused by OHR_{ext}, is a common feature under many typical OFR operation conditions. Peng et al. (2016) systematically examined the relative importance of non-OH (including non-tropospheric) reactants in the fate of VOCs over a wide range of conditions and provided guidelines for OFR operation to avoid non-tropospheric VOC photolysis, i.e., VOC photolysis at 185 and 254 nm.

In previous OFR modeling studies, NO_x chemistry was not investigated in detail since in such in typical OFR experiments with large amounts of oxidants (e.g., OH, HO₂, and O₃) NO would be very rapidly oxidized and thus unable to compete with HO₂ for reaction with peroxy radicals (RO₂). Li et al. (2015) estimated an NO (NO₂) lifetime of ~0.5 (~1.5) s under a typical OFR condition. From these estimates, OFRs processing ambient air or laboratory air without a large addition of NO_x were assumed to not be suitable for studying oxidation mechanisms relevant to polluted conditions under higher NO concentrations. OFRs have recently been used to conduct laboratory experiments with very high initial NO_x levels (Liu et al., 2015) and deployed to an urban tunnel where NO_x was high enough to be a major OH reactant (Tkacik et al., 2014). The former study reported evidence for the incorporation of nitrogen into SOA. OFRs have also been increasingly employed to process emissions of vehicles, biomass burning, and other combustion sources (Table 1) in which NO can often be hundreds of ppm (Ortega et al., 2013; Martinsson et al., 2015; Karjalainen et al., 2016; Link et al., 2016; Schill et al., 2016; Alanen et al., 2017; Simonen et al., 2017). It can be expected that such a high NO input together with very high VOC concentrations would cause a substantial deviation from the good OFR operation conditions identified in Peng et al. (2016). Very recently, N₂O injection has been proposed by Lambe et al. (2017) as a way to study the oxidation of VOCs under high NO conditions in an OFR. As more OFR studies at high NO_x levels are conducted, there is a growing need to understand the chemistry of N-containing species in OFRs and whether it proceeds along atmospherically relevant channels.

In this study, we present the first comprehensive model of OFR NO_y chemistry. We extend the model of Li et al. (2015) and Peng et al. (2015) by including a scheme for NO_y species. Then this model is used to investigate (i) whether an OFR with initial NO injection results in NO significantly reacting with RO₂ under any conditions, (ii) whether previously published OFR experiments with high initial NO concentrations led to RO₂+NO being dominant in VOC oxidation without negative side effects (e.g., non-tropospheric reactions), and (iii) how to avoid undesired chemistry in future studies. The results can provide insights into the design and

Table 1. Experimental conditions of several OFR studies with high NO injection.

Study	Source type	Temperature (K)	Relative humidity (%)	Dilution factor	External OH reactivity of undiluted source (s ⁻¹)	Source NO _x concentration (ppm)
Link et al. (2016)	Diesel vehicle emission		50	45–110	~ 5000 ¹	436 ¹
Martinsson et al. (2015)	Biomass burning emission			1700	156 400 ¹	154
Karjalainen et al. (2016)	Gasoline vehicle emission	295	60	12	~ 73 000 ^{2,a}	~ 400 ^{1,b}
Liu et al. (2015)	Purified gas	293	13	1	~ 1400 ^{1,a}	10 ^{1,b}
Tkacik et al. (2014)	Tunnel air	293	42	1	~ 60 ^{1,a}	~ 0.8 ¹
Ortega et al. (2013)	Biomass burning emission	290	30	~ 500	~ 250 000 ¹	~ 0.2

¹ Maximum value in the study; ² value at the moment of maximum NO emission; ^a NO_y species excluded; ^b NO only.

interpretation of future OH-oxidation OFR experiments with large amounts of NO_x injection.

2 Methods

The physical design of the OFR modeled in the present work, the chemical kinetics box model, and the method of propagating and analyzing the parametric uncertainties on the model have already been introduced previously (Kang et al., 2007; Li et al., 2015; Peng et al., 2015). We only provide brief descriptions for them below.

2.1 Potential aerosol mass flow reactor

The OFR modeled in this study is the potential aerosol mass (PAM) flow reactor first introduced by Kang et al. (2007). The PAM OFR is a cylindrical vessel with a volume of ~ 13 L, equipped with low-pressure Hg lamps (model no. 82-9304-03; BHK Inc.) to generate 185 and 254 nm UV light. This popular design is being used by many atmospheric chemistry research groups, particularly those studying SOA (Lambe and Jimenez, 2017 and references therein). When the lamps are mounted inside Teflon sleeves, photons at both wavelengths are transmitted and contribute to OH production (OFR185 mode). In OFR185, H₂O photolyzed at 185 nm produces OH and HO₂, while O₂ photolyzed at the same wavelengths results in O₃ formation. O(¹D) is produced via O₃ photolysis at 254 nm and generates additional OH through its reaction with H₂O. The 185 nm lamp emissions can be filtered by mounting the lamps inside quartz sleeves, leaving only 254 nm photons to produce OH (OFR254 mode). In this mode, injection of externally formed O₃ is necessary to ensure OH production. As the amount of O₃ injected is a key parameter under some conditions (Peng et al., 2015), we adopt the notation OFR254-X to denote OFR254 experiments with X ppm initial O₃ (O_{3,in}). In this study, we investigate OFR experiments with NO injected and thus utilize “OFR185-iNO” to describe the OFR185 mode of operation with initially (at the reactor entrance) injected NO.

The same terminology is used for the OFR254 mode. For instance, the initial NO injection into OFR254-7 is denoted as OFR254-7-iNO.

2.2 Model description

The basic framework of the box model used in this study, a standard chemical kinetics model, is the same as in Peng et al. (2015). Plug flow is assumed in the model, since approximately taking residence time distribution into account leads to similar results under most conditions but at much higher computational expense (Peng et al., 2015). In addition to the reactions in the model of Peng et al. (2015) including all HO_x reactions available in the JPL Chemical Kinetic Data Evaluation (Sander et al., 2011), all gas-phase NO_y reactions available in the JPL database except those of organic nitrates and peroxy nitrates are also considered in the current reaction scheme. An updated JPL evaluation was published recently (Burkholder et al., 2015) with slightly different (~ 20 %) rate constants for NO₂ + HO₂ + M → HO₂NO₂ + M and NO₂ + NO₃ → N₂O₅. The updated rate constants only result in changes of ~ 10–20 % in the concentrations of the species directly consumed or produced by these reactions. These changes are smaller than the parametric uncertainties of the model (see Sect. 3.1.3). For other species, concentration changes are negligible. HO₂NO₂ + M → HO₂ + NO₂ + M and N₂O₅ + M → NO₂ + NO₃ + M, are also included in the scheme with kinetic parameters from the IUPAC Task Group on Atmospheric Chemical Kinetic Data Evaluation (Ammann et al., 2016). As in Peng et al. (2015, 2016), SO₂ is used as a surrogate for external OH reactants (e.g., VOCs). NO_y species, although also external OH reactants, are explicitly treated in the model and *not* counted in OHR_{ext} in this work. Therefore, OHR_{ext} stands for *non*-NO_y OHR_{ext} only hereinafter unless otherwise stated.

Also, particle-phase chemistry and physical and chemical interactions of gas-phase species with particles are not considered in this study. We have made this assumption because of the following.

- i. The presence of aerosols has typically negligible impacts on the gas-phase chemistry of radicals, NO_y , and the OH reactants studied here. The condensational sink (CS) of ambient aerosols can rarely exceed 1 s^{-1} even in polluted areas and is usually 1–3 orders of magnitude lower (Donahue et al., 2016; Palm et al., 2016). Thus, even under the assumption of unity uptake coefficient, CS cannot compete with OHR_{ext} (usually on the order of 10 s^{-1} or higher) in OH loss. Uptake of NO onto aerosols only occurs through the reaction with RO_2 on the particle surface (Richards-Henderson et al., 2015), which is formed very slowly (see below) compared to gas-phase HO_x and NO_x chemistry. Uptake of HO_2 , O_3 , NO_3 , etc. is even more unlikely to be of importance due to lower uptake coefficients (Moise and Rudich, 2002; Moise et al., 2002; Hearn and Smith, 2004; Lakey et al., 2015). Combustion exhausts can have high aerosol loadings with condensational sinks on the order of 10^2 – 10^3 s^{-1} (Matti Maricq, 2007). Even if these exhausts are directly injected into the reactor without any pretreatment, uptake onto the particles still cannot play a major role in the fate of gas-phase radical and NO_x species since VOCs and NO_x in raw exhausts, which are proportionally orders of magnitude higher, still dominate the fate of oxidants. Dilution of combustion emissions simultaneously lowers condensational sinks and the sinks of oxidants due to chemical reactions with their relative importance remaining the same as in undiluted emissions.
- ii. Gas-phase radical and NO_y species only has limited impacts on OA chemistry in this study. The heterogeneous oxidation of OA by OH is generally slow. Significant OA loss due to heterogeneous oxidation can only be seen at photochemical ages as high as weeks (Hu et al., 2016). The enhancement of heterogeneous oxidation due to NO is remarkable only at OH concentrations close to the ambient values but not at typical values in an OFR (Richards-Henderson et al., 2015).

It is well known that the aerosol concentration can have a major impact on the physical uptake of semivolatile and low-volatility gas-phase species. However, this process is not explicitly modeled in this study.

As OHR_{ext} plays a major and even dominant role in OH loss, it is an important approximation that the *real* OHR_{ext} decay (due to primary VOC oxidation and subsequent oxidation of higher-generation products) is surrogated by that of SO_2 (see Fig. S2 of Peng et al., 2015). Gas-phase measurements in the literature on laboratory studies revealed that there is large variability in the evolution of total OHR_{ext} during the oxidation of primary VOCs and subsequent oxidation of their intermediate products depending on the type of precursors (Nehr et al., 2014; Schwantes et al., 2017). This variability is clearly mainly due to the formation of different types and amounts of oxidation intermediates and products

contributing to OHR_{ext} . This variation is highly complex due to the large number of possible oxidation intermediates and the limited knowledge of detailed higher-generation mechanisms, and thus it is difficult to accurately capture even if modeling with a mechanism as explicit as the Master Chemical Mechanism (Schwantes et al., 2017). Therefore, it is justified to use a lumped surrogate to model the OHR_{ext} decay for simplicity and efficiency. This approximation is a substantial contributor to the uncertainty in our model. The uncertainties due to the types of oxidation intermediates and products are very likely larger than those due to mass transfer processes between gas and particle phases, wall losses, etc., which are not considered in this study.

A residence time of 180 s and the typical temperature (295 K) and atmospheric pressure (835 mbar) in Boulder, CO, USA are assumed for all model cases. The lower-than-sea-level pressure only leads to minor differences in the outputs (Li et al., 2015). We explore physical input cases evenly spaced in a logarithmic scale over very wide ranges: H_2O of 0.07–2.3 %, i.e., relative humidity (RH) of 2–71 % at 295 K; 185 nm UV of 1.0×10^{11} – 1.0×10^{14} and 254 nm UV of 4.2×10^{13} – 8.5×10^{15} photons $\text{cm}^{-2} \text{ s}^{-1}$; OHR_{ext} of 1–16000 s^{-1} ; $\text{O}_{3,\text{in}}$ of 2.2–70 ppm for OFR254; and initial NO mixing ratio (NO^{in}) from 10 ppt to 40 ppm. Conditions with $\text{OHR}_{\text{ext}} = 0$ are also explored. UV at 254 nm is estimated from that at 185 nm according to the relationship determined by Li et al. (2015). Several typical cases within this range and their corresponding four- or two-character labels (e.g., MM0V and HL) are defined in Table 2. Literature studies are modeled by adopting all reported parameters (e.g., residence time, H_2O , and $\text{O}_{3,\text{in}}$) and estimating any others that may be needed (e.g., UV) from the information provided in the papers.

In this study, OH equivalent ages are calculated under the assumption of an ambient OH concentration of 1.5×10^6 molecules cm^{-3} (Mao et al., 2009). Conditions leading to a ratio of RO_2 reacted with NO over the entire residence time [$r(\text{RO}_2 + \text{NO})$] to that with HO_2 [$r(\text{RO}_2 + \text{HO}_2)$] larger than 1 are regarded as “high NO” (under the assumption of constant OHR_{ext} from VOCs; see Sect. S1 for more details), where [$r(X)$] is the total reactive flux for reaction X over the entire residence time. $\text{F}_{185\text{exp}}/\text{OH}_{\text{exp}}$ and $\text{F}_{254\text{exp}}/\text{OH}_{\text{exp}}$ are used as measures of the relative importance of VOC photolysis at 185 and 254 nm to their reactions with OH, respectively; $\text{F}_{185\text{exp}}$ ($\text{F}_{254\text{exp}}$) are 185 (254) nm photon flux exposure, i.e., the product of 185 (254) nm photon flux and time. Readers may refer to Figs. 1 and 2 of Peng et al. (2016) for the determination of the relative importance of non-tropospheric (185 and 254 nm) photolysis of individual VOCs. Although the relative importance of non-tropospheric photolysis depends on individual VOCs, in the present work, we set criteria on $\text{F}_{185\text{exp}}/\text{OH}_{\text{exp}} < 3 \times 10^3 \text{ cm s}^{-1}$ and $\text{F}_{254\text{exp}}/\text{OH}_{\text{exp}} < 4 \times 10^5 \text{ cm s}^{-1}$ to define “good” conditions and $\text{F}_{185\text{exp}}/\text{OH}_{\text{exp}} < 1 \times 10^5 \text{ cm s}^{-1}$ and

Table 2. Code of the labels of typical cases. A case label can be composed of four characters denoting the water mixing ratio, the photon flux, the external OH reactivity excluding N-containing species, and the initial NO mixing ratio. A case label can also be composed of two characters denoting the water mixing ratio and the photon flux.

	Water mixing ratio	Photon flux	External OH reactivity (no ON)	Initial NO mixing ratio
Options	<i>L</i> = low (0.07 %)	<i>L</i> = low (10^{11} photons $\text{cm}^{-2} \text{s}^{-1}$ at 185 nm; 4.2×10^{13} photons $\text{cm}^{-2} \text{s}^{-1}$ at 254 nm)	0	0
	<i>M</i> = medium (1 %)	<i>M</i> = medium (10^{13} photons $\text{cm}^{-2} \text{s}^{-1}$ at 185 nm; 1.4×10^{15} photons $\text{cm}^{-2} \text{s}^{-1}$ at 254 nm)	<i>L</i> = low (10 s^{-1})	<i>L</i> = low (10 ppb)
	<i>H</i> = high (2.3 %)	<i>H</i> = high (10^{14} photons $\text{cm}^{-2} \text{s}^{-1}$ at 185 nm; 8.5×10^{15} photons $\text{cm}^{-2} \text{s}^{-1}$ at 254 nm)	<i>H</i> = high (100 s^{-1})	<i>H</i> = high (316 ppb)
			<i>V</i> = very high (1000 s^{-1})	<i>V</i> = very high (10 ppm)
Example	LH0V:	low water mixing ratio, high photon flux, no external OH reactivity (excluding ON), very high initial NO mixing ratio		
	ML:	medium water mixing ratio, low photon flux		

Table 3. Definition of condition types in this study (good/risky/bad high-/low-NO conditions).

Condition	Good	Risky	Bad
Criterion	$F_{185_{\text{exp}}}/OH_{\text{exp}} < 3 \times 10^3 \text{ cm s}^{-1}$ and $F_{254_{\text{exp}}}/OH_{\text{exp}} < 4 \times 10^5 \text{ cm s}^{-1}$	$F_{185_{\text{exp}}}/OH_{\text{exp}} < 1 \times 10^5 \text{ cm s}^{-1}$ and $F_{254_{\text{exp}}}/OH_{\text{exp}} < 1 \times 10^7 \text{ cm s}^{-1}$ (excluding good conditions)	$F_{185_{\text{exp}}}/OH_{\text{exp}} \geq 1 \times 10^5 \text{ cm s}^{-1}$ or $F_{254_{\text{exp}}}/OH_{\text{exp}} \geq 1 \times 10^7 \text{ cm s}^{-1}$
Condition	High NO	Low NO	
Criterion*	$\frac{r(\text{RO}_2+\text{NO})}{r(\text{RO}_2+\text{HO}_2)} > 1$	$\frac{r(\text{RO}_2+\text{NO})}{r(\text{RO}_2+\text{HO}_2)} \leq 1$	

* See Sect. S1 for details.

$F_{254_{\text{exp}}}/OH_{\text{exp}} < 1 \times 10^7 \text{ cm s}^{-1}$ (excluding good conditions) to define “risky” conditions. Conditions with higher $F_{185_{\text{exp}}}/OH_{\text{exp}}$ or $F_{254_{\text{exp}}}/OH_{\text{exp}}$ are defined as “bad”. Under good conditions, the photolysis of most VOCs has a relative contribution $< 20\%$ to their fate; under bad conditions, non-tropospheric photolysis is likely to be significant in all OFR experiments since it can hardly be avoided for oxidation intermediates, even if the precursor(s) does not photolyze at all. Under risky conditions, some species photolyzing slowly and/or reacting with OH rapidly (e.g., alkanes, aldehydes, and most biogenics) still have a relative photolysis contribution of $< 20\%$ to their fates, while species photolyzing more rapidly and/or reacting with OH more slowly (e.g., aromatics and other highly conjugated species and some saturated carbonyls) will undergo substantial non-tropospheric photolysis. Note that these definitions are slightly different than in Peng et al. (2016). All definitions of the types of conditions are summarized in Table 3.

2.3 Uncertainty analysis

We apply the same method as in Peng et al. (2014, 2015) to calculate and analyze the output uncertainties due to uncertain kinetic parameters in the model. Random samples following lognormal distributions are generated for all rate constants and photoabsorption cross sections in the model using uncertainty data available in the JPL database (Sander et al., 2011) or estimated based on IUPAC data (Ammann et al., 2016). Then, Monte Carlo uncertainty propagation (BIPM et al., 2008) is performed for these samples through the model to obtain the distributions of outputs. Finally, we compute squared correlation coefficients between corresponding input and output samples and apportion the relative contributions of individual kinetic parameters to the output uncertainties based on these coefficients (Saltelli et al., 2005).

3 Results and discussion

In this section, we study the NO_y chemistry in an OFR while considering relevant experimental issues. Based on these results, we propose some guidelines for OFR operation for high-NO OH oxidation of VOCs.

3.1 NO_y chemistry in typical OFR cases with initial NO injection

NO was thought to be unimportant (i.e., unable to significantly react with RO_2) in OFRs with initial NO injection (OFR-iNO) based on the argument that its lifetime is too short due to large amounts of O_3 , OH, and HO_2 to compete with $\text{RO}_2 + \text{HO}_2$ (Li et al., 2015). We evaluate this issue below by calculating NO effective lifetime (τ_{NO} ; in s), defined as NO exposure (NO_{exp} , in molecules cm^{-3} s) divided by initial NO concentration, under various conditions. This definition cannot effectively capture the true NO average lifetime if it is close to or longer than the residence time. In this case, τ_{NO} close to the residence time will be obtained, which is still long enough for our characterization purposes.

3.1.1 OFR185-iNO

In OFR185-iNO, NO is *not* oxidized extremely quickly under *all* conditions. For instance, under a typical condition in the midrange of the phase space shown in Fig. 1a, $\tau_{\text{NO}} \sim 13$ s. This lifetime is much shorter than the residence time but long enough for OH_{exp} to reach $\sim 3 \times 10^{10}$ molecules cm^{-3} s, which is equivalent to an OH equivalent age of ~ 6 h. Such an OH equivalent age is already sufficient to allow some VOC processing and even SOA formation to occur (Lambe et al., 2011; Ortega et al., 2016). Within τ_{NO} , NO suppresses HO_2 through the reaction $\text{NO} + \text{HO}_2 \rightarrow \text{NO}_2 + \text{OH}$, leading to $\text{NO}_{\text{exp}}/\text{HO}_{2\text{exp}}$ of ~ 700 during this period, which is high enough for RO_2 to dominantly react with NO. Meanwhile, $\text{NO} + \text{HO}_2 \rightarrow \text{NO}_2 + \text{OH}$ enhances OH production, which helps OH_{exp} build up in a relatively short period. In addition, non-tropospheric photolysis of VOCs at 185 and 254 nm is minor ($\text{F}_{185\text{exp}}/\text{OH}_{\text{exp}} \sim 600 \text{ cm s}^{-1}$, Fig. 1a) because of enhanced OH production and moderate UV. Therefore, such an OFR condition may be of some interest for high-NO VOC oxidation. We thus analyze the NO_y chemistry in OFR185-iNO in more detail below by taking the case shown in Fig. 1a as a representative example.

In OFR185-iNO, HO_x concentrations are orders of magnitude higher than in the atmosphere, while the amount of O_3 produced is relatively small during the first several seconds after the flow enters the reactor. As a result, NO is not oxidized almost exclusively by O_3 as in the troposphere, but also by OH and HO_2 to form HONO and NO_2 , respectively (Fig. 1a). The large concentration of OH present then oxidizes HONO to NO_2 and NO_2 to HNO_3 . Photolysis only plays a negligible role in the fate of HONO and NO_2 in OFRs

in contrast to the troposphere where it is the main fate of these species. This is because the reactions of HONO and NO_2 with OH are greatly accelerated in OFR compared to those in the troposphere, while photolysis not (Peng et al., 2016). The interconversion between NO_2 and HO_2NO_2 is also greatly accelerated (Fig. 1a) since a large amount of HO_2 promotes the formation of HO_2NO_2 , the reaction with OH and thermal decomposition of which in turn enhance the recycling of NO_2 . Though not explicitly modeled in this study, RO_2 is expected to undergo similar reactions with NO_2 to form reservoir species, i.e., peroxy nitrates (Orlando and Tyndall, 2012). Peroxy nitrates that decompose on timescales considerably longer than OFR residence times may serve as effectively permanent NO_y sinks in OFRs (see Sect. 3.4.1).

Interestingly but not surprisingly, the NO_y chemistry shown in Fig. 1a is far from temporally uniform during the OFR residence time (Fig. S1a in the Supplement). Within τ_{NO} , NO undergoes an e-fold decay as it is rapidly converted into NO_2 and HONO with concentrations that reach maxima around that time. After most NO is consumed, HONO and NO_2 also start to decrease, but significantly more slowly than NO, since they do not have as many or efficient loss pathways as NO. The reaction of OH with HONO, the dominant fate of HONO, is slower than that with NO (Fig. 1a). The net rate of the NO_2 -to- HO_2NO_2 conversion becomes low because of the relatively fast reverse reaction (Fig. 1a). The total loss of NO_2 is also partially offset by the production from HONO. The generally stable concentrations of HONO and NO_2 (Fig. S1a) result in their respective reaction rates with OH that are comparable during and after τ_{NO} (Fig. 1a), as OH variation is also relatively small during the entire residence time (Fig. S1b). However, the NO_2 -to- HO_2NO_2 conversion after τ_{NO} is much faster than during it (Fig. 1a) as a result of substantially decreased NO and HO_2 concomitantly increasing by > 1 order of magnitude after τ_{NO} (Fig. S1a and b). HNO_3 and HO_2NO_2 , which are substantially produced only after NO_2 is built up, have much higher concentrations later than within τ_{NO} .

Under other OFR185-iNO conditions than in Fig. 1a, the major reactions interconverting NO_y species are generally the same, although their relative importance may vary. At lower NO^{in} , the perturbation of HO_x chemistry caused by NO_y species is smaller. The effects of NO^{in} less than 1 ppb (e.g., typical non-urban ambient concentrations) are generally negligible regarding HO_x chemistry. Regarding NO_y species, the pathways in Fig. 1a are still important under those conditions. At higher NO^{in} (e.g., > 1 ppm), one might expect NO_3 and N_2O_5 to play a role (as in OFR254-iNO; see Sect. 3.1.2 below) since high NO_y concentrations might enhance self- or cross- reactions of NO_y . However, this would not occur unless OH production is high since relatively low O_3 concentrations in OFR185-iNO cannot oxidize NO_2 to NO_3 rapidly. Also, a large amount of NO_y can lead to significant OH suppression. That would in turn slow down the NO_3 production from HNO_3 by OH. This is especially true

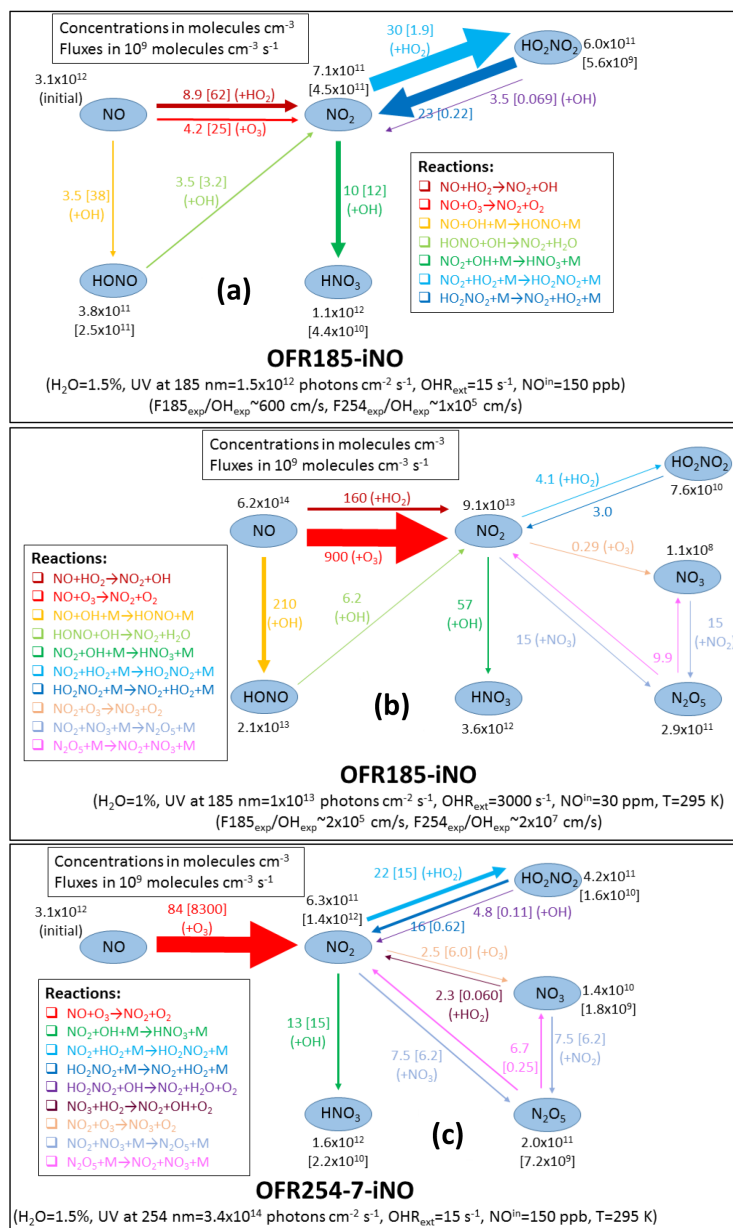


Figure 1. Schematics of main N-containing species and their major interconversion pathways under typical input conditions for (a) OFR185-iNO with $\text{NO}^{\text{in}} = 150 \text{ ppb}$, (b) OFR254-7-iNO with $\text{NO}^{\text{in}} = 150 \text{ ppb}$, and (c) OFR185-iNO with $\text{NO}^{\text{in}} = 30 \text{ ppm}$. Species average concentrations (in molecules cm^{-3}) are shown in black beside species names. Arrows denote directions of the conversions. Average reaction fluxes (in units of $10^9 \text{ molecules cm}^{-3} \text{ s}^{-1}$) are calculated according to the production rate and shown on or beside the corresponding arrows and in the same color. Within each schematic, the thickness of the arrows is a measure of their corresponding species flux. Multiple arrows in the same color and pointing to the same species should be counted only once for reaction flux on a species. Note that all values in these schematics are average ones over the residence time, except for those in square brackets in panels (a) and (b), which are average values within approximate NO effective lifetime (τ_{NO} , or more accurately, an integer multiple of the model's output time step closest to NO effective lifetime). All concentrations and fluxes have two significant digits.

when an OFR is used to oxidize the output of highly concentrated sources (e.g., from vehicle exhausts). When sources corresponding to OHR_{ext} of thousands of s^{-1} and NO^{in} of tens of ppm are injected into OFR185 (Fig. 1b), they essentially inhibit active chemistry except NO consumption, as all

subsequent products are much less abundant compared to remaining NO (Fig. S1c).

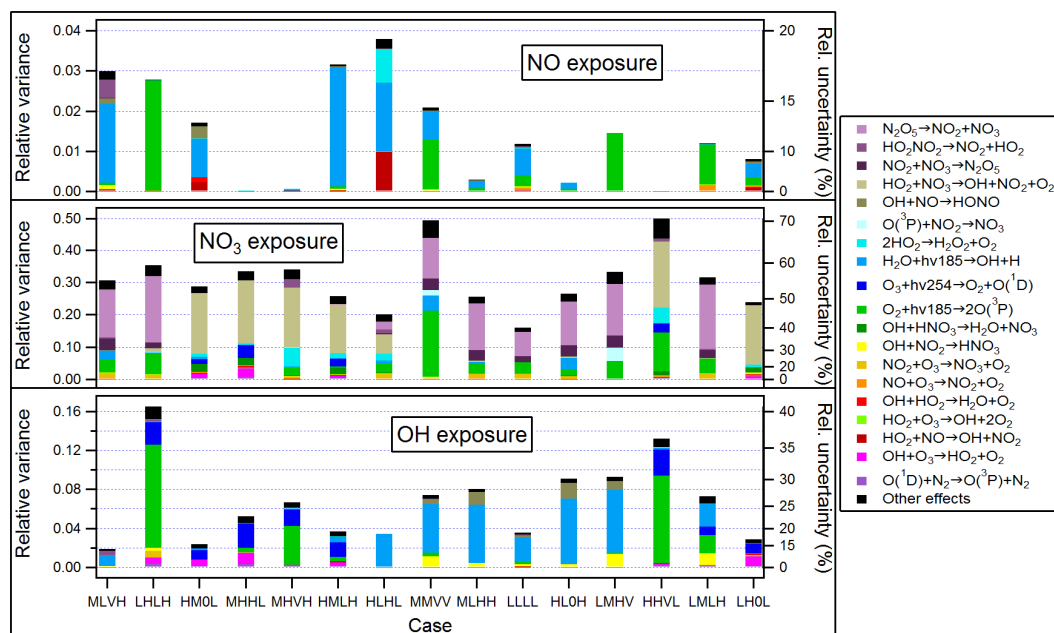


Figure 2. Relative variances (left axes) and uncertainties (right axes) in several outputs (i.e., NO, NO₃, and OH exposures) of Monte Carlo uncertainty propagation and relative contributions of key reactions to these relative variances in several typical cases (denoted in four-character labels; see Table 2 for the typical case label code) in OFR185-iNO. Relative variances are shown in linear scales (left axis), while corresponding relative uncertainties equal to relative variances' square roots are indicated by the nonlinear right axis. Only the reactions with a contribution of no less than 0.04 to at least one relative variance are shown.

3.1.2 OFR254-iNO

The ppm level $O_{3,\text{in}}$ used in the OFR254-iNO mode of operation has a strong impact on its NO_y chemistry. An $O_{3,\text{in}}$ of 2.2 ppm (lowest in this study) is already enough to shorten τ_{NO} to ~ 1 s, preventing NO from playing a role in the chemistry under most explored conditions. The reaction fluxes under a typical $O_{3,\text{in}}$ of 7 ppm are shown in Fig. 1c. A reactive flux from $\text{NO} + \text{O}_3 \rightarrow \text{NO}_2$ makes the reaction of NO with other oxidants (OH, HO₂, etc.) negligible. The HNO₃ production pathway from NO₂ is similar to that in OFR185-iNO. The interconversion between NO₂ and HO₂NO₂ is also fast over the residence time and even faster than in OFR185-iNO during τ_{NO} since a high concentration of O₃ also controls the OH–HO₂ interconversion and makes HO₂ more resilient against suppression due to high NO (Fig. S1f; Peng et al., 2015). A major difference in the NO_y chemistry in OFR254-iNO (Fig. 1c) compared to OFR185-iNO (Fig. 1a) is significant NO₃/N₂O₅ chemistry due to high O₃ in OFR254-iNO, which accelerates the oxidation of NO₂ to NO₃. Interconversion between NO₂ + NO₃ and N₂O₅ also occurs to a significant extent because of high NO₂. Under the conditions of Fig. 1c, NO₃ can also be significantly consumed by HO₂. Unlike OFR185-iNO, OFR254-iNO can substantially form NO₃ from HNO₃ under conditions that are not on the extremes of the explored physical condition space, e.g., at higher UV and lower NOⁱⁿ (e.g., Fig. S2). In the case of very high NOⁱⁿ

(equal to or higher than $O_{3,\text{in}}$), all O₃ can be rapidly destroyed by NO. As a consequence, OH production is shut down and these cases are of little practical interest (Fig. S3h).

3.1.3 Uncertainty analysis

The results of uncertainty propagation confirm that the output uncertainties due to uncertain kinetic parameters are relatively low compared to other factors (e.g., non-plug flow in OFR; Peng et al., 2015) and the overall model accuracy compared to experimental data (a factor of 2–3; Li et al., 2015). For OFR185-iNO, NO, NO₃, and OH exposures have relative uncertainties of ~ 0 –20, ~ 40 –70, and ~ 15 –40 %, respectively. The uncertainties in OH exposure are very similar to those in the cases without NO_x (Peng et al., 2015). The contribution of NO_y reactions to OH_{exp} uncertainty is negligible, except for some contribution of OH + NO → HONO in a few cases with high NOⁱⁿ (Fig. 2). The uncertainties in NO_{exp} are dominated by the reactions producing HO_x and O₃, i.e., the major consumers of NO. For NO₃ exposure, a few major production and loss pathways (e.g., $\text{NO}_2 + \text{NO}_3 \rightarrow \text{N}_2\text{O}_5$, $\text{N}_2\text{O}_5 \rightarrow \text{NO}_2 + \text{NO}_3$, and $\text{HO}_2 + \text{NO}_3 \rightarrow \text{OH} + \text{NO}_2 + \text{O}_2$) dominate its uncertainties. OFR254-iNO has a simpler picture of parametric uncertainties in terms of composition. O₃ controls the NO oxidation under most conditions and this reaction contributes most of the output uncertainties for NO exposures. $\text{HO}_2 + \text{NO}_3 \rightarrow \text{OH} + \text{NO}_2 + \text{O}_2$ dominates the uncertainty in NO₃ exposure. The levels of those uncertain-

ties are lower than in OFR185-iNO (< 2 % for NO exposure, < 60 % in all cases, and < 25 % in most cases for NO₃ exposure). Thus, model uncertainties in OFR254-iNO are not shown in detail.

3.2 Different conditions types

Having illustrated the main NO_y chemical pathways for typical cases, we present the results of the exploration of the entire physical parameter space (see Sect. 2.2). Note that the explored space is indeed very large and gridded logarithmically uniformly in every dimension. Therefore, the statistics of the exploration results can be useful to determine the relative importance of the condition types defined in Sect. 2.2 and Table 3.

It has been shown that during τ_{NO} , RO₂ can react dominantly with NO (Sect. 3.1.1), while the entire residence time is considered to determine if a condition is high-NO (see Table 3). This is done because for VOC oxidation systems of interest, there will be significant oxidation of the initial VOC and its products under low-NO conditions if τ_{NO} is shorter than the reactor residence time. After most NO is consumed, the longer the remaining residence time, the more RO₂ will react with HO₂ and the more likely that an input condition is classified as low NO. For a condition to be high NO, a significantly long τ_{NO} is required. Figure 3 shows the fractional occurrence distribution of good, risky, and bad conditions in the entire explored condition space over logarithm of $r(\text{RO}_2+\text{NO})/r(\text{RO}_2+\text{HO}_2)$, which distinguishes high- and low-NO conditions. In OFR254-iNO, τ_{NO} is so short that no good high-NO condition is found in the explored range in this study (Fig. 3a). A fraction of explored conditions are bad high-NO. These conditions result from a full consumption of O₃ by NO. Then very little HO_x is produced (right panels in Fig. S3h), but the fate of any RO₂ formed is dominated by RO₂ + NO (right panels in Fig. S3i). However, also due to negligibly low OH concentration, little RO₂ is produced and non-tropospheric photolysis of VOCs is also substantial compared to their reaction with OH under these conditions, classifying all of them as “bad” (Fig. 3a).

In OFR185-iNO, in addition to the typical case shown in Fig. 1a, many other cases have a τ_{NO} of ~ 10 s or longer (Figs. S3b and S4), which allows for the possibility of high-NO conditions. Indeed, $\sim 1/3$ of explored conditions in OFR185-iNO with a residence time of 3 min are high NO (Fig. 3b). Most of these high-NO conditions are also classified as bad, similar to those in OFR254-iNO. More importantly, in contrast to OFR254-iNO, good and risky high-NO conditions also comprise an appreciable fraction of the OFR185-iNO conditions. It is easily expected that very high OHR_{ext} and NOⁱⁿ lead to bad high-NO conditions (all panels in Fig. 4) since they strongly suppress HO_x, which yields bad conditions and in turn keeps NO destruction relatively low. The occurrence of bad high-NO conditions is reduced at high UV (bottom panels in Fig. 4), which can be explained by

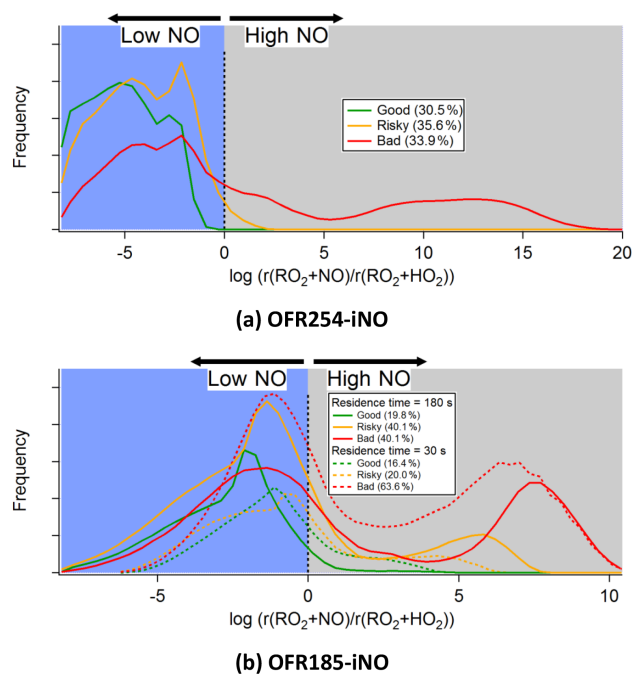


Figure 3. Frequency occurrence distributions of good, risky, and bad conditions (see Table 3) over logarithm of the ratio between RO₂ reacted with NO and with HO₂ (see Sect. S1 for more detail) for (a) OFR254-iNO (only the case with a residence time of 180 s) and (b) OFR185-iNO (including two cases with residence times of 180 and 30 s). Low- and high-NO regions (see Table 3) are colored in light blue and gray, respectively.

lowered NO due to high O₃ production and fast OH reactant loss due to high OH production. Good high-NO conditions are rare in the explored space. They are only 1.1 % of total explored conditions (Fig. 3b) and present under very specific conditions, i.e., higher H₂O, lower UV, lower OHR_{ext}, and NOⁱⁿ of tens to hundreds of ppb (Figs. 4 and S5). Since a very high NO can suppress OH, to obtain both a significant NO level and good conditions, NOⁱⁿ can only be tens to hundreds of ppb. As NOⁱⁿ is lower and OH is higher than under bad high-NO conditions, UV should be lower than bad high-NO conditions to keep a sufficiently long presence of NO. Thus, UV levels at 185 nm for good high-NO conditions are generally lower than 10^{12} photons cm⁻² s⁻¹ (Fig. S5). In addition, a low OHR_{ext} (generally < 50 s⁻¹) and a higher H₂O (the higher the better, although there is no apparent threshold) are also required for good high-NO conditions (Fig. S5), as Peng et al. (2016) pointed out. Risky high-NO conditions often occur between good and bad high-NO conditions, e.g., at lower NOⁱⁿ than bad conditions (e.g., Cases ML, MM, HL, and HM in Fig. 4; see Table 2 for the typical case label code), at higher OHR_{ext} and/or NOⁱⁿ than good conditions (e.g., Cases ML and MM), and at lower H₂O than good conditions (e.g., Case LL).

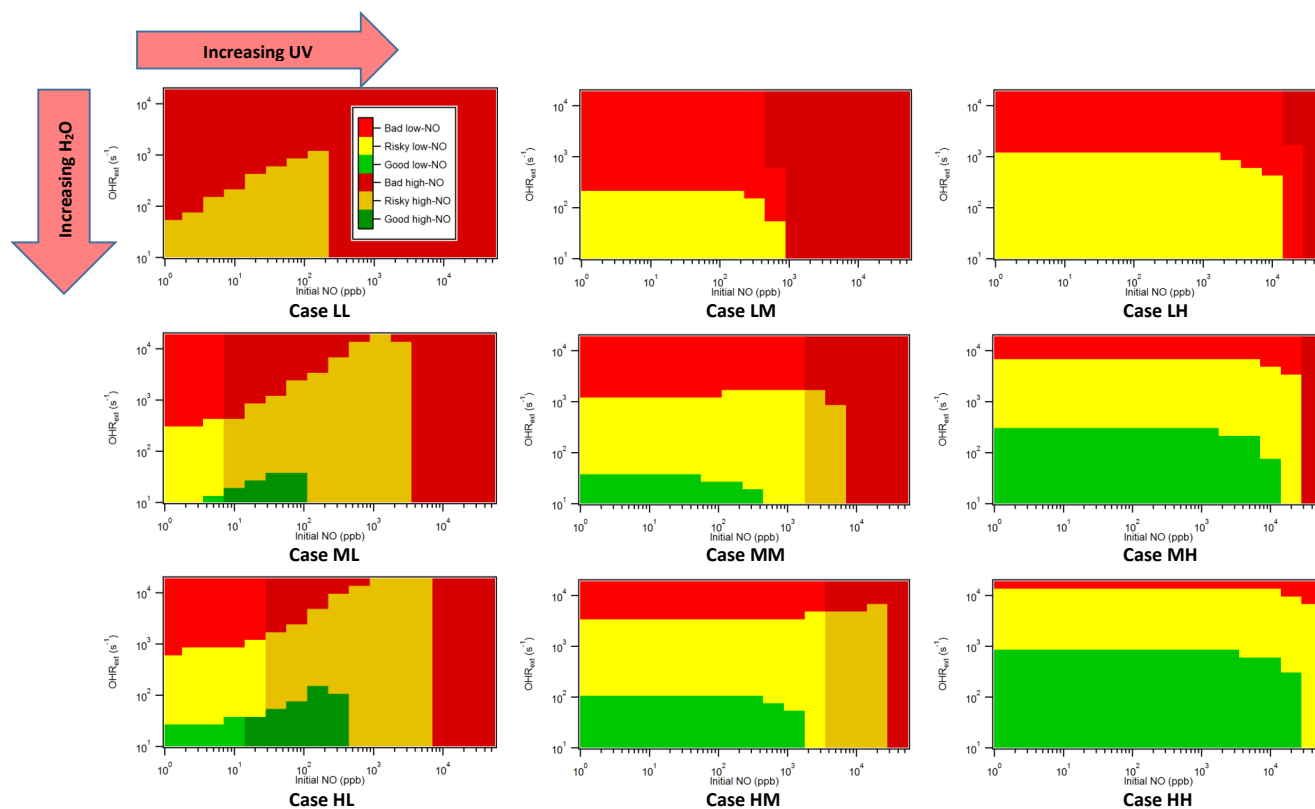


Figure 4. Image plots of the condition types defined in Table 3 vs. external OH reactivity (excluding N-containing species) and initial NO for several typical cases in OFR185-iNO (see Table 2 for the case label code).

The trend in the distributions of good, risky, and bad low-NO conditions is generally in line with the analysis in Peng et al. (2016). For low-NO conditions, NO_y species can be simply regarded as external OH reactants, as in Peng et al. (2016). As H_2O decreases and/or OHR_{ext} or NO^{in} increases, a low-NO condition becomes worse (good \rightarrow risky \rightarrow bad; Figs. 4 and 5). In OFR185-iNO, increasing UV generally makes a low-NO condition better because of an OH production enhancement (Fig. 4), while in OFR254-iNO, increasing UV generally makes a low-NO condition worse (Fig. 5) since at a higher UV more O_3 is destroyed and the resilience of OH to suppression is reduced.

As discussed above, the fraction of high-NO conditions also depends on OFR residence time. A shorter residence time is expected to generally lead to a larger fraction of high-NO conditions since the time spent in the reaction for $t > \tau_{\text{NO}}$ is significantly smaller. Thus, we also investigate an OFR185-iNO case with a residence time of 30 s. In Fig. 3b, compared to the case with a residence time of 3 min, the distributions of all condition types (good, risky, and bad) of the 30 s residence time case shift toward higher $r(\text{RO}_2 + \text{NO})/r(\text{RO}_2 + \text{HO}_2)$. Nevertheless, shortening the residence time also removes the period when the condition is better (i.e., less non-tropospheric photolysis), when external OH reactants have been partially consumed, and

OH suppression due to OHR_{ext} has been reduced later in the residence time. As a result, the fractions of good and risky conditions decrease (Fig. 3b). With the two effects (higher $r(\text{RO}_2 + \text{NO})/r(\text{RO}_2 + \text{HO}_2)$ and more significant non-tropospheric photolysis) combined, the fraction of good high-NO conditions increases by a factor of ~ 3 . An even shorter residence time does not result in a larger good high-NO fraction since the effect of enhancing non-tropospheric photolysis is even more apparent.

3.3 Effect of non-plug flow

We performed model runs in which the only change with respect to our box model introduced in Sect. 2.2 is that the plug flow assumption is replaced by the residence time distribution (RTD) measured by Lambe et al. (2011; see also Fig. S8 of Peng et al., 2015). The chemistry of different air parcels with different residence times is simulated by our box model and outputs are averaged over the RTD. Lateral diffusion between different air parcels is neglected in these simulations.

OH_{exp} calculated from the mode with RTD ($\text{OH}_{\text{exp,RTD}}$) is higher than that calculated from the plug flow model ($\text{OH}_{\text{exp,PF}}$) in both OFR185-iNO and OFR254-iNO (Table 4 and Fig. S6). Under most explored conditions deviations are relatively small, which leads to an overall posi-

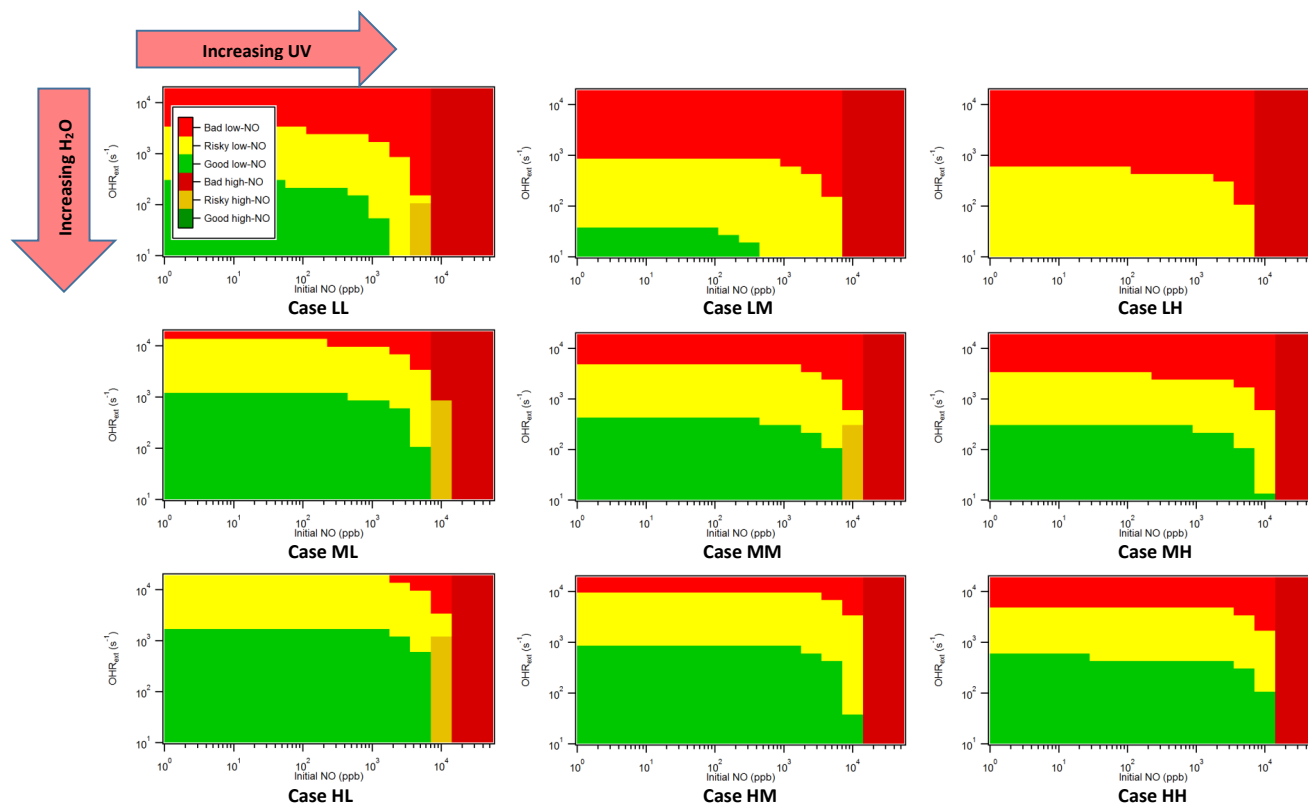


Figure 5. Same format as Fig. 4 but for OFR254-22-iNO.

tive deviation of $\text{OH}_{\text{exp,RTD}}$ from $\text{OH}_{\text{exp,PF}}$ by $\sim \times 2$ (within the uncertainties of the model and its application to real experimental systems). For OFR185-iNO, most conditions ($\sim 90\%$) in the explored space lead to $< \times 3$ differences between $\text{OH}_{\text{exp,PF}}$ and $\text{OH}_{\text{exp,RTD}}$, while for a small fraction of cases the differences can be larger (Fig. S6). The larger deviations are mainly present at high UV, OHR_{ext} , and NO^{in} in which conditions are generally bad and in which experiments are of little atmospheric relevance. Under these specific conditions, external OH reactants and NO_y can be substantially destroyed for the air parcels with residence times longer than the average, while this is not the case for the average residence time. This feature was already described by Peng et al. (2015; see Fig. S10 of that study). Although only non- NO_y external OH reactants were considered in that study, the results are the same. In the present study, a higher upper limit of the explored OHR_{ext} range (compared to Peng et al., 2015, due to trying to simulate the extremely high OHR_{ext} used in some recent literature studies) leads to large amounts of NO_y and causes somewhat larger deviations. In OFR254-iNO, OH is less suppressed at high OHR_{ext} and NO^{in} than in OFR185-iNO because of high O_3 (Peng et al., 2015); $\text{OH}_{\text{exp,RTD}}$ deviations from $\text{OH}_{\text{exp,PF}}$ are also smaller (Table 4).

Based on the outputs of the model with RTD, a similar mapping of the physical input space as in Figs. 4 and 5 can be done (Figs. S7 and S8). Overall, the mapping of

Table 4. Statistics of the ratio between OH exposures calculated in the model with the Lambe et al. (2011) residence time distribution ($\text{OH}_{\text{exp,RTD}}$) and in the plug flow model ($\text{OH}_{\text{exp,PF}}$). The geometric mean, uncertainty factor (geometric standard deviation), and percentage of outlier cases (> 3 or $< 1/3$) are shown for OFR185-iNO, OFR254-70-iNO, and OFR254-7-iNO.

	Geometric mean	Uncertainty factor	Outlier cases (%)
OFR185-iNO	1.91	1.64	11
OFR254-7-iNO	1.59	1.51	7
OFR254-70-iNO	1.48	1.29	3

the RTD model results is very similar to that of the plug flow model. The conditions appear to be only slightly better in a few places of the explored space than those from the plug flow model, which can be easily explained by the discussions above. The mapping in Figs. S7 and S8 also appear to be slightly more low NO for the same reasons discussed above. After NO is destroyed at long residence times, HO_2 suppressed by NO also recovers as OH, and $r(\text{RO}_2 + \text{NO})/r(\text{RO}_2 + \text{HO}_2)$ is clearly expected to be smaller than in the plug flow model in general.

Note that most conditions that appear to be better in the RTD model results are already identified as bad by the plug flow model. Those conditions look slightly better only because of their better *RTD-averaged* $F185_{\text{exp}}/\text{OH}_{\text{exp}}$ and $F254_{\text{exp}}/\text{OH}_{\text{exp}}$. However, each of those cases is actually composed of both a better part at longer residence times and also a worse part at shorter residence times. Under those conditions, the reactor simultaneously works in two distinct regimes, one of which is bad due to heavy OH suppression. Such conditions are clearly not desirable for OFR operation.

3.4 Possible issues related to high NO_x levels

In the discussion above, we focused on obtaining high-NO conditions and considered only one experimental issue (non-tropospheric photolysis) that had been previously investigated in Peng et al. (2016) and is not specific for experiments with high NO injection. We discuss additional potential reasons why the OFR-iNO chemistry can deviate strongly from tropospheric conditions as specifically related to high NO_x levels in this subsection.

3.4.1 NO_2

NO_2 reacts with RO_2 to form peroxy nitrates, which are generally regarded as reservoir species in the atmosphere as most of them thermally decompose very quickly compared to atmospheric timescales. However, in OFRs with residence times on the order of minutes, some peroxy nitrates may no longer be considered as fast decomposing. This is especially true for acylperoxy nitrates with lifetimes that can be hours at room temperature (Orlando and Tyndall, 2012). Acylperoxy nitrates are essentially sinks instead of reservoirs in OFRs for both NO_2 and RO_2 . RO_2 is estimated to be as high as several ppb in OFRs by our model (e.g., ~ 6 ppb RO_2 in OFR185 at $\text{H}_2\text{O} = 1\%$, UV at 185 nm = 1×10^{13} photons $\text{cm}^{-2} \text{s}^{-1}$, $\text{OHR}_{\text{ext}} = 1000 \text{s}^{-1}$, and $\text{NO}^{\text{in}} = 0$), while high-NO experiments can yield far higher NO_2 . If all RO_2 were acylperoxy, the RO_2 chemistry could be rapidly shut down by NO_2 , as rate constants of these $\text{RO}_2 + \text{NO}_2$ reactions are around $10^{-11} \text{cm}^3 \text{molecule}^{-1} \text{s}^{-1}$ (Orlando and Tyndall, 2012). Nevertheless, acyl peroxy nitrates are not expected to typically be the dominant component of peroxy nitrates since acyl radicals are not a direct oxidation product of most common VOCs and can only be formed after several steps of oxidation (Atkinson and Arey, 2003; Ziemann and Atkinson, 2012). Most alkylperoxy nitrates retain their short-lived reservoir characteristics in OFRs due to their relatively short thermal decomposition timescales (on the order of 0.1 s; Orlando and Tyndall, 2012). Even so, OFR experiments can be seriously hampered at extremely high NO_2 . If NO_2 reaches ppm levels, the equilibrium between $\text{RO}_2 + \text{NO}_2$ and alkylperoxy nitrate ($\text{RO}_2 + \text{NO}_2 \leftrightarrow \text{RO}_2\text{NO}_2$) is greatly shifted toward the alkylperoxy nitrate side, as the forward and reverse rate con-

stants are on the order of $10^{-12} \text{cm}^3 \text{molecule}^{-1} \text{s}^{-1}$ and 1s^{-1} , respectively (Orlando and Tyndall, 2012). This results in a substantial decrease in effective RO_2 concentration, or in other words, a substantial slowdown of RO_2 chemistry.

Parts per million levels of NO_2 may impose an additional experimental artifact in the oxidation chemistry of aromatic precursors. OH–aromatic adducts, i.e., the immediate products of aromatic oxidation by OH, undergo the addition of O_2 and NO_2 at comparable rates under ppm levels of NO_2 (rate constants of the additions of O_2 and NO_2 are on the order of 10^{-16} and 10^{-11} molecules $\text{cm}^{-3} \text{s}^{-1}$, respectively; Atkinson and Arey, 2003). However, only the former addition is atmospherically relevant (Calvert et al., 2002). Liu et al. (2015) performed OFR254-iNO experiments with toluene over a range of NO^{in} of 2.5–10 ppm, encompassing the NO concentration range at which the reactions of OH–toluene adduct with O_2 and with NO_2 are of equal importance (~ 5 ppm; Atkinson and Arey, 2003). This suggests that nitroaromatics, the formation of which was reported in the study of Liu et al. (2015), might have been formed in substantial amounts in that study through the addition of NO_2 to the OH–toluene adduct.

3.4.2 NO_3

As discussed in Sect. 3.1, NO_3 can be formed in significant amounts in OFRs with high NO injection. Although NO_3 is also present in the atmosphere, especially during nighttime, significant VOC oxidation by both OH and NO_3 results in more complex chemistry that may complicate the interpretation of experimental results. NO_3 oxidation-only OFRs have been previously realized experimentally via the thermal dissociation of injected N_2O_5 (Palm et al., 2017). We discuss below how to avoid significant VOC oxidation by NO_3 and achieve OH-dominated VOC oxidation in OFRs with high NO injection.

If $\text{NO}_{3\text{exp}}/\text{OH}_{\text{exp}} > 0.1$, NO_3 can be a competitive reactant for biogenic alkenes and dihydrofurans, which have a C–C bond for NO_3 addition, and phenols, which have activated hydroxyl for fast hydrogen abstraction by NO_3 (Atkinson and Arey, 2003). For lower $\text{NO}_{3\text{exp}}/\text{OH}_{\text{exp}}$, OH is expected to dominate the oxidation of all VOCs, as shown in Fig. 6. Oxidation for VOCs without alkene C–C bonds and phenol hydroxyl (such as alkanes and (alkyl)benzenes) is dominated by OH unless $\text{NO}_{3\text{exp}}/\text{OH}_{\text{exp}} > 1000$. Despite its double bond, ethene reacts as slowly with NO_3 as alkanes, likely due to lack of alkyl groups enriching the electron density on the C–C bond, which slows NO_3 addition. We calculate $\text{NO}_{3\text{exp}}/\text{OH}_{\text{exp}}$ for OFR185-iNO and OFR254-iNO and plot histograms of this ratio in Fig. 6. Many experimental conditions lead to high enough $\text{NO}_{3\text{exp}}/\text{OH}_{\text{exp}}$ that NO_3 is a competitive sink for alkenes, while only under very extreme conditions can NO_3 be a competitive sink for species without C–C bonds. High-NO conditions in OFR185-iNO have lower $\text{NO}_{3\text{exp}}/\text{OH}_{\text{exp}}$ ($\sim 10^{-2}$ – 10^2) than in OFR254-

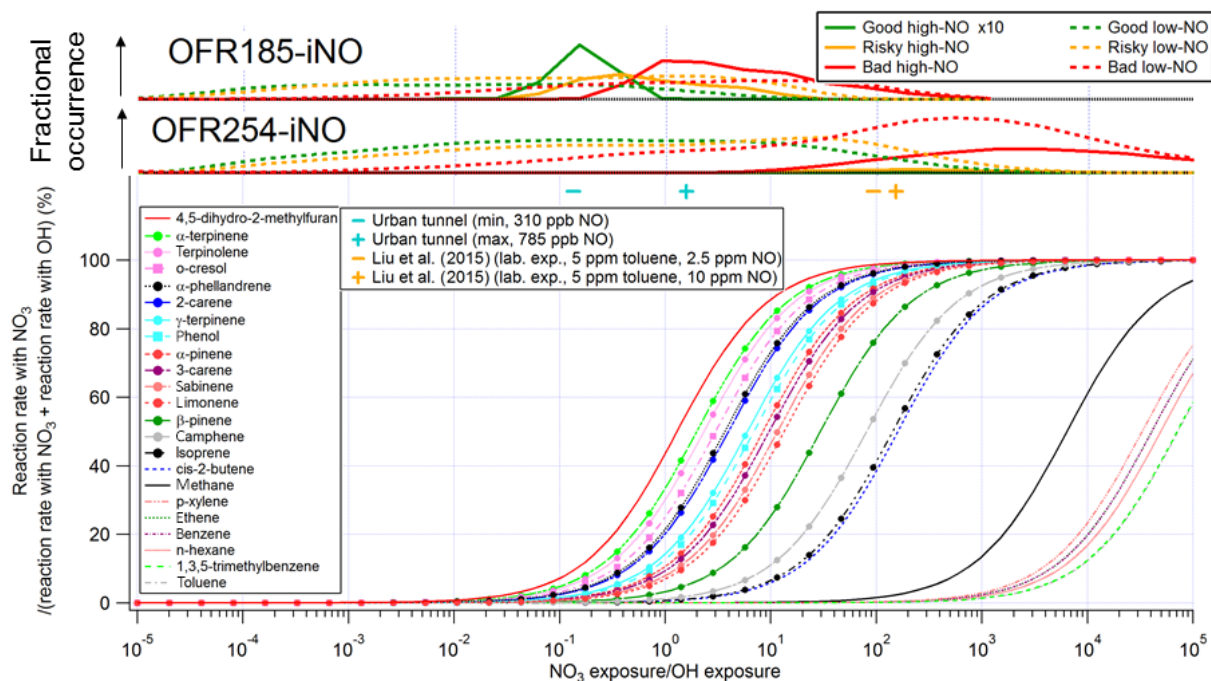


Figure 6. Fractional importance of the reaction rate of several species of interest with NO_3 vs. that with OH as a function of the ratio of exposure to NO_3 and OH. The curves of biogenics and phenols are highlighted by solid dots and squares, respectively. The turquoise and orange markers show the ranges of modeled exposure ratios between NO_3 and OH of a source study in an urban tunnel (Tkacik et al., 2014) and a laboratory study (Liu et al., 2015), respectively, using an OFR. In the upper part of the figure, the modeled frequency distributions of ratios of NO_3 exposure to OH exposure under good/risky/bad high-/low-NO conditions for OFR185-iNO and OFR254-iNO are also shown. See Table 3 for the definitions of the three types of conditions. All curves, markers, and histograms in this figure share the same abscissa.

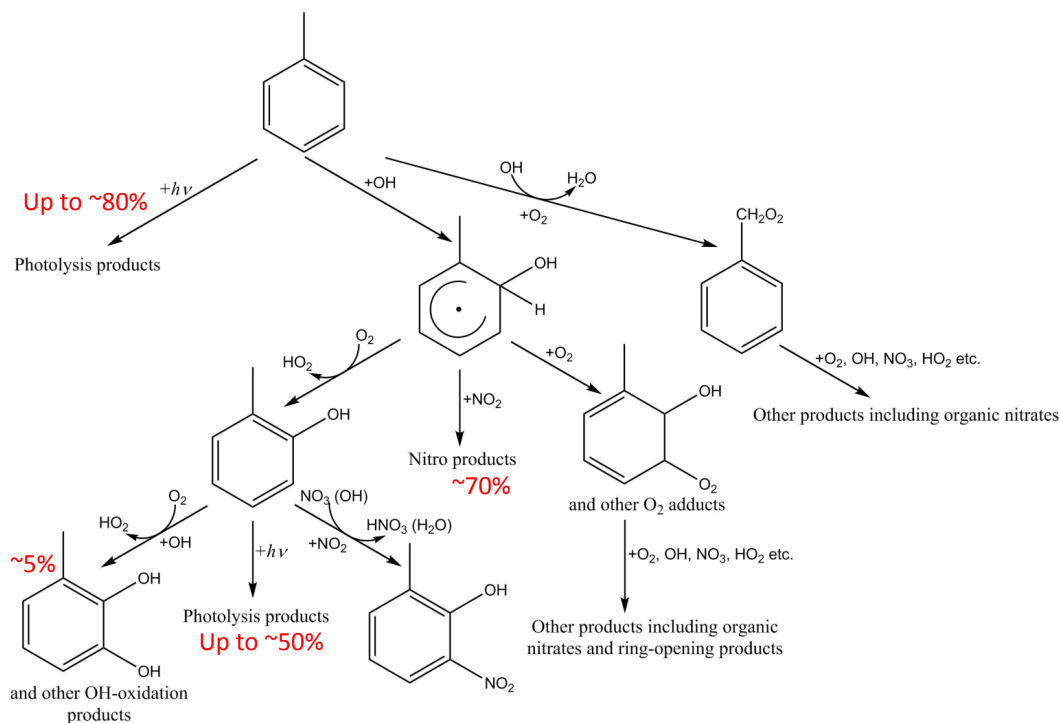
iNO ($\sim 10^1$ – 10^5) (Figs. 6 and S3d, g, j). This difference in $\text{NO}_{3\text{exp}}/\text{OH}_{\text{exp}}$ is due to the different levels of O_3 in the two modes, as high O_3 promotes NO_2 -to- NO_3 oxidation. Note that low-NO conditions in both OFR185-iNO and OFR254-iNO can also reach high $\text{NO}_{3\text{exp}}/\text{OH}_{\text{exp}}$ as some high-NO conditions have. This is because in OFR185-iNO a large part of NO_3 is formed by OH oxidation, resulting in $\text{NO}_{3\text{exp}}/\text{OH}_{\text{exp}}$ being largely influenced by NO^{in} but not by other factors mainly governing OH (Fig. S3d); under low-NO conditions in OFR254-iNO, NO_3 can form rapidly from $\text{NO}_2 + \text{O}_3$, while OH can be heavily suppressed by high OHR_{ext} (Fig. S3g and j).

Most of the species shown in Fig. 6 are primary VOCs, except phenols and a dihydrofuran, which can be intermediates of the atmospheric oxidation of (alkyl)benzenes (Atkinson and Arey, 2003) and long-chain alkanes (Aimanant and Ziemann, 2013; Strollo and Ziemann, 2013; Ranney and Ziemann, 2016), respectively. Nevertheless, only the phenol production may occur in high-NO OFRs, as the particle-phase reaction in the photochemical formation of dihydrofurans from alkanes is too slow compared to typical OFR residence times (Ranney and Ziemann, 2016). Therefore, the impact of NO_3 oxidation on VOC fate needs to be considered only if the OFR input flow contains high NO mixed with biogenics and/or aromatics, e.g., (alkyl)benzenes and/or phenols.

However, (alkyl)benzenes were likely to be major SOA precursors in, to our knowledge, the only literature OFR studies with high NO levels (Ortega et al., 2013; Tkacik et al., 2014; Liu et al., 2015). In the study of the air in a traffic tunnel (OFR185-iNO mode; Tkacik et al., 2014), where toluene is usually a major anthropogenic SOA precursor as in other urban environments (Dzepina et al., 2009; Borbon et al., 2013; Hayes et al., 2015; Jathar et al., 2015), NO_x was several hundred ppb. This resulted in an estimated $\text{NO}_{3\text{exp}}/\text{OH}_{\text{exp}}$ range of ~ 0.1 – 1 in which up to $\sim 30\%$ of cresols (intermediates of toluene oxidation) may have been consumed by NO_3 . Dihydrofurans may also have formed in the tunnel air (but outside the OFR) in the presence of NO_x (Aimanant and Ziemann, 2013; Strollo and Ziemann, 2013), and after entering the OFR they would have been substantially (up to $\sim 50\%$) consumed by NO_3 . In the laboratory experiment of Liu et al. (2015) with toluene, the injection of as much as 10 ppm of NO elevated $\text{NO}_{3\text{exp}}/\text{OH}_{\text{exp}}$ to ~ 100 , at which cresols from toluene oxidation reacted almost exclusively with NO_3 in addition to being photolyzed.

3.4.3 A case study

We use a case study of an OFR254-13-iNO laboratory experiment with a large amount of toluene (5 ppm) and NO^{in}



Scheme 1. Possible major reactions in an OFR254-13-iNO with 5 ppm toluene and 10 ppm initial NO. Branching ratios in red are estimated by the model and/or according to Calvert et al. (2002), Atkinson and Arey (2003), Ziemann and Atkinson (2012), and Peng et al. (2016). Note that addition or substitution on the aromatic ring may occur at other positions. Intermediates and products shown here are the isomers that are most likely to form. Branching ratios shown in red are not overall but from immediate reactant.

(10 ppm) to illustrate how very high VOC and NO concentrations cause multiple types of atmospherically irrelevant reactions in an OFR. Due to very high OHR_{ext} and NO^{in} , the photolysis of toluene at 254 nm may have been important (Peng et al., 2016). In the case of a high (close to 1) quantum yield, up to ~80% of the consumed toluene in their experiments could have been photolyzed (Scheme 1). Of the rest of reacted toluene, ~10% undergoes H abstraction by OH from the methyl group in the model, leading to an RO_2 similar to alkyl RO_2 and likely proceeding with normal RO_2 chemistry. Approximately 90% of the toluene formed an OH adduct (Calvert et al., 2002). As discussed above, 70% of this adduct (depending on NO^{in}) is predicted to recombine with NO_2 , producing nitroaromatics because of the ppm level NO_x . The adduct could also react with O_2 via two types of pathways, one of which was addition forming a special category of RO_2 (OH-toluene- O_2 adducts) potentially undergoing ring-opening (Atkinson and Arey, 2003; Orlando and Tyndall, 2012; Ziemann and Atkinson, 2012). The other was H elimination by O_2 , producing cresols. Again, like toluene, cresols may have been substantially photolyzed. As a result of $NO_{3exp}/OH_{exp} \sim 100$, only a minor portion of cresol could have undergone OH addition and then H elimination again. This pathway leads to the formation of methyl-dihydroxybenzenes and other OH-oxidation products (Atkinson and Arey,

2003). The rest of the cresols may have formed methylphenoxy radicals but nevertheless dominantly via H abstraction by NO_3 , since H abstraction by OH was a minor pathway compared to the OH-addition one (Atkinson et al., 1992). In summary, the model results suggest that there were two possible routes leading to nitroaromatic formation. However, one of them (recombination of OH-aromatic adducts with NO_2) is likely of little atmospheric relevance due to very high NO_x needed, and the other (H abstraction from cresol) occurs in the atmosphere but is not a major fate of aromatics (Calvert et al., 2002).

3.5 Implications for OFR experiments with combustion emissions as input

Emissions from combustion sources, e.g., vehicles and biomass burning, usually contain VOCs and NO_x at very high concentrations (Table 1). An injection of this type of emissions (typically with OHR_{ext} of thousands of s^{-1} or larger and NO^{in} of tens of ppm or larger) in OFRs without any pretreatment is likely to cause all experimental issues discussed in Peng et al. (2016) and this paper, i.e., strong OH suppression, substantial non-tropospheric photolysis, strong RO_2 suppression by NO_2 whether RO_2 is acyl RO_2 or not, fast reactions of NO_2 with OH-aromatic hydrocarbon adducts, substantial NO_3 contribution to VOC fate,

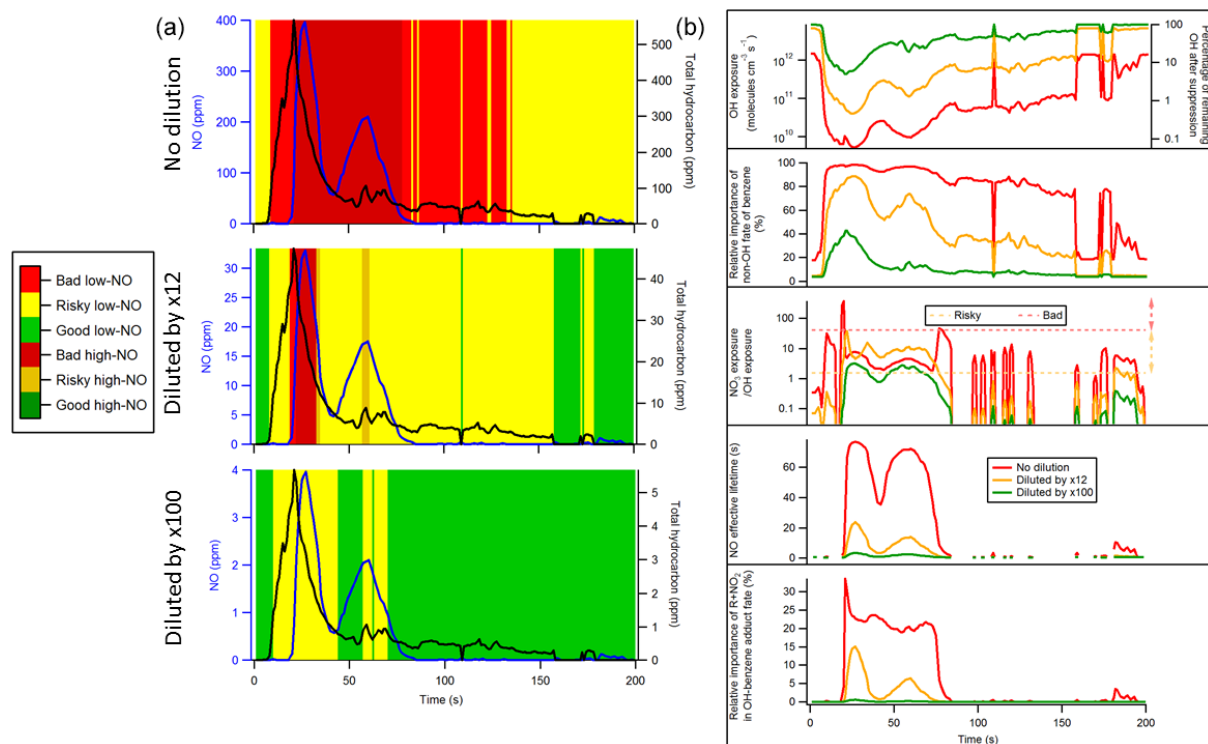


Figure 7. (a) NO and total hydrocarbon during the first 200 s of the test of Karjalainen et al. (2016) in the cases of no dilution, dilution by a factor of 12 (as actually done in that study), and dilution by a factor of 100. Different periods of time are colored according to corresponding emissions (i.e., input conditions for OFR) classified as good/risky/bad high-/low-NO emissions. (b) OH exposure and percentage of remaining OH after suppression, relative importance of non-OH fate of benzene, exposure ratio of NO_3 to OH, NO effective lifetime, and relative importance of reaction of OH–toluene adduct with NO_2 in the fate of this adduct in the OFR of Karjalainen et al. (2016) during the first 200 s of their test in the cases of no dilution, dilution by a factor of 12, and dilution by a factor of 100. Horizontal orange and red dashed lines in the middle right panel denote “risky” and “bad” regions for exposure ratio of NO_3 to OH, respectively. Above the orange (red) dashed line, reaction with NO_3 contributes $> 20\%$ to the fate of phenol (isoprene).

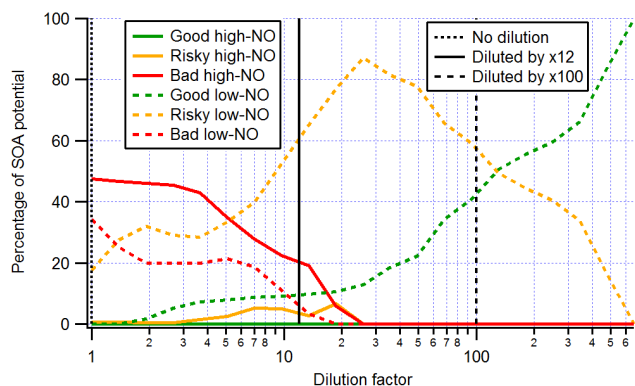


Figure 8. Secondary organic aerosol (SOA) potential (estimated from the total hydrocarbon measurement) in the OFR of Karjalainen et al. (2016) formed during periods of time in the OFR corresponding to good/risky/bad high-/low-NO conditions as a function of dilution factor. Vertical lines denoting dilution factors of 1, 12 (as actually used in that study), and 100 are also shown.

and even a nearly total inhibition of OFR chemistry due to complete titration of O_3 by NO in the case of OFR254. We take the study of Karjalainen et al. (2016), who used an OFR to oxidize diluted car exhaust in real time, as a case study to investigate the extent to which these issues may affect typical combustion source studies and to explore approaches to mitigate the problems.

During the first 200 s of their experiment (defined as the “cold start” period when the catalyst is cold and emissions are high), NO and total hydrocarbon in the emissions of the test vehicle reached ~ 400 and ~ 600 ppm, respectively. We first simulate the oxidation of those emissions without any dilution (even though $\times 12$ dilution was used in their experiments) to explore the most extreme conditions. Our model simulation indicates that such an extremely concentrated source would generally lead to bad high- or low-NO conditions (depending on NO concentration) in their OFR (Fig. 7), even though it was run at relatively high H_2O and UV. OH suppression can be as high as 3 orders of magnitude, VOC fates by non-tropospheric photolysis and reactions of alkenes and phenols with NO_3 can be nearly 100%,

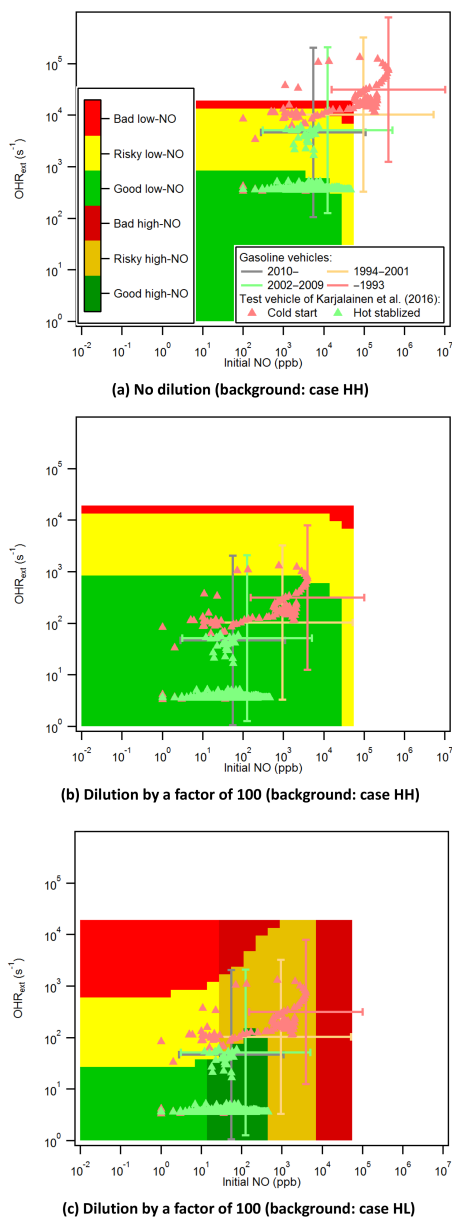


Figure 9. Location of individual 1 s data points vs. OFR185-iNO reaction conditions. Data points are shown from the test vehicle of Karjalainen et al. (2016) and average exhaust from gasoline vehicle on-road emissions measured by Bishop and Stedman (2013). On-road emissions are classified by vehicle year and the distribution of each category is shown as a cross representing 1 SD (standard deviation; with lognormal distribution assumed). The x and y axes are NO and external OH reactivity (excluding N-containing species) due to vehicle emissions in an OFR in the cases of (a) no dilution and (b, c) dilution by a factor of 100. The Karjalainen et al. (2016) points are classified as cold start (during the first 200 s) and hot stabilized (during 200–1000 s). In addition, the same image plots as the panels of cases HH (high H_2O and high UV; see Table 2 for the case label code) and HL in Fig. 4 (OFR185-iNO) are shown as background for comparison.

and up to $\sim 1/3$ of OH–toluene adduct may be recombined with NO_2 instead of forming an adduct with O_2 . After the test vehicle entered the “hot stabilized” stage (200–1000 s), its VOC emissions (on the order of ppm) were still too high for an undiluted OFR to yield a good condition (Fig. S9). OH suppression can still reach 2 orders of magnitude, non-tropospheric photolysis and sometimes reactions with NO_3 can still dominate over reactions with OH in VOC fates, and reactions of OH–toluene adduct with NO_2 can still be substantial at some small NO emission spikes. Moreover, although NO emissions were roughly at ppm level even during the hot stabilized period, the NO effective lifetime may be very short during that period, leading to low-NO conditions in their OFR.

As suggested in Peng et al. (2016) for a low-NO OFR, the dilution of sources can also mitigate strong deviations in OFR-iNO chemistry vs. atmospherically relevant conditions. A dilution by a factor of 12, as actually used by Karjalainen et al. (2016), appears to be sufficient to bring most of the hot stabilized period under good conditions (Fig. S9). However, most VOC, or in other words most SOA formation potential, was emitted during the cold start period when risky and bad conditions still prevailed (Figs. 7 and 8). Even if the emissions are diluted by $\times 100$, the cold-start emission peak (Fig. 7) is still under risky conditions. Although bad conditions are eliminated and a good condition is present most of time, this emission peak under risky conditions may contribute $> 50\%$ to total SOA formation potential (Fig. 8). For SOA formed under good condition to be dominant, a dilution factor of > 400 would be needed. Note that a strong dilution lowers aerosol mass loading in vehicle emissions. As a result, the condensation of gases onto particles is slower than in raw exhausts. However, condensational sinks after dilution may still be significantly higher than typical ambient values (Matti Maricq, 2007; Donahue et al., 2016).

Note that the emissions of the test vehicle of Karjalainen et al. (2016) are rather clean compared to the typical 2013 US on-road fleet (i.e., all at the hot stabilized stage) measured by Bishop and Stedman (2013; Figs. 9 and S10). For the emissions of an average on-road fleet, a dilution by a factor of 100 or larger would be necessary to ensure that most emissions are processed in OFR185 under good conditions at the highest H_2O and UV in this study (Figs. 9b and S10b, e, h). In the case of lower H_2O and/or UV, an even larger dilution factor would be required.

Conducting OFR185-iNO experiments at high UV lowers the dilution factor needed for good conditions. However, it also renders good high-NO conditions impossible (see Sect. 3.2 and Fig. S4). If one wants to oxidize vehicle exhausts in a high-NO environment in an OFR, as in an urban atmosphere, OFR185 at low UV is necessary. Consequently, a much stronger dilution is in turn necessary to keep the operation conditions good. Nevertheless, not all vehicle emissions can be moved into the good high-NO region through a simple dilution (Figs. 9c and S10c, f, i). Further-

more, a low UV would seriously limit the highest OH_{exp} that OFRs can achieve ($\sim 3 \times 10^{11}$ molecules cm^{-3} s for modeled good high-NO conditions in this study), while a much higher OH_{exp} would be desirable to fully convert SOA formation potential into measurable SOA mass. If both good high-NO conditions and high OH_{exp} are required, new techniques (e.g., injection of N_2O at the percent level as proposed by Lambe et al., 2017) may be necessary.

4 Conclusions

In this study, OFR chemistry involving NO_y species was systematically investigated over a wide range of conditions. NO initially injected into the OFR was found to be rapidly oxidized under most conditions. In particular, due to high O_3 concentrations, the NO lifetime in OFR254-iNO was too short to result in significant RO_2 consumption by NO compared to that by HO_2 under all conditions with active chemistry. Nevertheless, it is not completely impossible for OFR185-iNO to have a significant RO_2 fate by NO and minor non-tropospheric photolysis at the same time (good high-NO conditions). According to our simulations, these conditions are most likely present at high H_2O , low UV, low OHR_{ext} , and NO^{in} of tens to hundreds of ppb.

However, many past OFR studies with high NO injection were conducted under conditions remarkably different from the abovementioned very narrow range. NO^{in} and/or OHR_{ext} in those studies were often much higher than good high-NO conditions require (particularly, > 3 orders of magnitude in some OFR studies using combustion emissions as input). In addition to non-tropospheric organic photolysis, OFR oxidation of highly concentrated sources can cause multiple large deviations from tropospheric OH oxidation, i.e., RO_2 suppression by high NO_2 , substantial nitroaromatic formation from the recombination of NO_2 and OH–aromatic adducts, and fast reactions of VOCs with NO_3 compared to those with OH.

Working at lower NO_x (sub ppm level) and VOC concentrations or dilution can mitigate these experimental problems. In general, a strong dilution (by a factor of > 100) is needed for an OFR that processes typical on-road vehicle emissions. Humidification can also make good conditions more likely. By using these measures, good conditions can be guaranteed as long as NO and/or precursor concentrations are sufficiently low, while high-NO conditions cannot be ensured. To aid the design and interpretation of OFR experiments with high NO injection, we provide our detailed modeling results in a visualized form (Fig. S3). For OFR users in need of both high OH_{exp} and high NO, simple NO injection is not a good option. New techniques (e.g., the injection of N_2O as proposed by Lambe et al. (2017) or other innovations) may be necessary to meet this need.

Data availability. The model outputs in this study are available from the authors upon request (jose.jimenez@colorado.edu). All data shown in the figures in this paper (including the Supplement) can be downloaded from http://cires1.colorado.edu/jimenez/group_pubs.html.

The Supplement related to this article is available online at <https://doi.org/10.5194/acp-17-11991-2017-supplement>.

Competing interests. The authors declare that they have no conflict of interest.

Acknowledgements. This work was partially supported by DOE (BER/ASR) DE-SC0011105 and DE-SC0016559, EPA STAR 83587701-0, and NSF AGS-1360834. We thank Pengfei Liu, Andrew Lambe, and Daniel Tkacik for providing some OFR experimental data, the authors of Karjalainen et al. (2016) and their project IEA-AMF Annex 44 for providing the data and information for the vehicle tests, Gary Bishop for providing on-road vehicle emission data, and Andrew Lambe and William Brune for useful discussions.

Edited by: Dwayne Heard

Reviewed by: Gordon McFiggans and one anonymous referee

References

- Aimantant, S. and Ziemann, P. J.: Chemical Mechanisms of Aging of Aerosol Formed from the Reaction of n-Pentadecane with OH Radicals in the Presence of NO_x , *Aerosol Sci. Tech.*, 47, 979–990, <https://doi.org/10.1080/02786826.2013.804621>, 2013.
- Alanen, J., Simonen, P., Saarikoski, S., Timonen, H., Kangasniemi, O., Saukko, E., Hillamo, R., Lehtoranta, K., Murtonen, T., Vesala, H., Keskinen, J., and Rönkkö, T.: Comparison of primary and secondary particle formation from natural gas engine exhaust and of their volatility characteristics, *Atmos. Chem. Phys. Discuss.*, <https://doi.org/10.5194/acp-2017-44>, in review, 2017.
- Ammann, M., Cox, R. A., Crowley, J. N., Jenkin, M. E., Mellouki, A., Rossi, M. J., Troe, J., Wallington, T. J., Cox, B., Atkinson, R., Baulch, D. L., and Kerr, J. A.: IUPAC Task Group on Atmospheric Chemical Kinetic Data Evaluation, available at: <http://iupac.pole-ether.fr/#> (last access: February 2017), 2016.
- Atkinson, R. and Arey, J.: Atmospheric degradation of volatile organic compounds, *Chem. Rev.*, 103, 4605–4638, <https://doi.org/10.1021/cr0206420>, 2003.
- Atkinson, R., Aschmann, S. M., and Arey, J.: Reactions of hydroxyl and nitrogen trioxide radicals with phenol, cresols, and 2-nitrophenol at 296 ± 2 K, *Environ. Sci. Technol.*, 26, 1397–1403, <https://doi.org/10.1021/es00031a018>, 1992.
- BIPM, IEC, IFCC, ILAC, ISO, IUPAC and IUPAPOIML: JCGM 101: 2008 Evaluation of measurement data – Supplement 1 to the “Guide to the expression of uncertainty in measurement” – Propagation of distributions using a Monte

- Carlo method, http://www.bipm.org/utis/common/documents/jcgm/JCGM_101_2008_E.pdf (last access: December 2016), 2008.
- Bishop, G. A. and Stedman, D. H.: Fuel Efficiency Automobile Test: Light-Duty Vehicles, available at: http://www.feat.biochem.du.edu/light_duty_vehicles.html (last access: 1 February 2017), 2013.
- Borbon, A., Gilman, J. B., Kuster, W. C., Grand, N., Chevaillier, S., Colomb, A., Dolgorouky, C., Gros, V., Lopez, M., Sarda-Estevé, R., Holloway, J., Stutz, J., Petetin, H., McKeen, S., Beekmann, M., Warneke, C., Parrish, D. D., and De Gouw, J. A.: Emission ratios of anthropogenic volatile organic compounds in northern mid-latitude megacities: Observations versus emission inventories in Los Angeles and Paris, *J. Geophys. Res.-Atmos.*, 118, 2041–2057, <https://doi.org/10.1002/jgrd.50059>, 2013.
- Burkholder, J. B., Sander, S. P., Abbatt, J., Barker, J. R., Huie, R. E., Kolb, C. E., Kurylo, M. J., Orkin, V. L., Wilmouth, D. M., and Wine, P. H.: Chemical Kinetics and Photochemical Data for Use in Atmospheric Studies, Evaluation Number 18, Pasadena, CA, USA, available at: <http://jpldataeval.jpl.nasa.gov/> (last access: February 2017), 2015.
- Calvert, J. G., Atkinson, R., Becker, K. H., Kamens, R. M., Seinfeld, J. H., Wallington, T. H., and Yarwood, G.: The Mechanisms of Atmospheric Oxidation of the Aromatic Hydrocarbons, Oxford University Press, USA, available at: <https://books.google.com/books?id=P0basalrxDMC> (last access: February 2017), 2002.
- Carlton, A. G., Wiedinmyer, C., and Kroll, J. H.: A review of Secondary Organic Aerosol (SOA) formation from isoprene, *Atmos. Chem. Phys.*, 9, 4987–5005, <https://doi.org/10.5194/acp-9-4987-2009>, 2009.
- Carter, W. P. L., Cocker, D. R., Fitz, D. R., Malkina, I. L., Bumiller, K., Sauer, C. G., Pisano, J. T., Bufalino, C., and Song, C.: A new environmental chamber for evaluation of gas-phase chemical mechanisms and secondary aerosol formation, *Atmos. Environ.*, 39, 7768–7788, <https://doi.org/10.1016/j.atmosenv.2005.08.040>, 2005.
- Chameides, W., Lindsay, R., Richardson, J., and Kiang, C.: The role of biogenic hydrocarbons in urban photochemical smog: Atlanta as a case study, *Science*, 241, 1473–1475, <https://doi.org/10.1126/science.3420404>, 1988.
- Cocker, D. R., Flagan, R. C., and Seinfeld, J. H.: State-of-the-Art Chamber Facility for Studying Atmospheric Aerosol Chemistry, *Environ. Sci. Technol.*, 35, 2594–2601, <https://doi.org/10.1021/es0019169>, 2001.
- Donahue, N. M., Posner, L. N., Westervelt, D. M., Li, Z., Shrivastava, M., Presto, A. A., Sullivan, R. C., Adams, P. J., Pandis, S. N., and Robinson, A. L.: Where Did This Particle Come From? Sources of Particle Number and Mass for Human Exposure Estimates, in: *Airborne Particulate Matter: Sources, Atmospheric Processes and Health*, edited by: Harrison, R. M., Hester, R. E., and Querol, X., Royal Society of Chemistry, Cambridge, UK, 35–71, 2016.
- Dzepina, K., Volkamer, R. M., Madronich, S., Tulet, P., Ulbrich, I. M., Zhang, Q., Cappa, C. D., Ziemann, P. J., and Jimenez, J. L.: Evaluation of recently-proposed secondary organic aerosol models for a case study in Mexico City, *Atmos. Chem. Phys.*, 9, 5681–5709, <https://doi.org/10.5194/acp-9-5681-2009>, 2009.
- George, I. J., Vlasenko, A., Slowik, J. G., Broekhuizen, K., and Abbatt, J. P. D.: Heterogeneous oxidation of saturated organic aerosols by hydroxyl radicals: uptake kinetics, condensed-phase products, and particle size change, *Atmos. Chem. Phys.*, 7, 4187–4201, <https://doi.org/10.5194/acp-7-4187-2007>, 2007.
- Haagen-Smit, A. J.: Chemistry and Physiology of Los Angeles Smog, *Ind. Eng. Chem.*, 44, 1342–1346, <https://doi.org/10.1021/ie50510a045>, 1952.
- Hallquist, M., Wenger, J. C., Baltensperger, U., Rudich, Y., Simpson, D., Claeys, M., Dommen, J., Donahue, N. M., George, C., Goldstein, A. H., Hamilton, J. F., Herrmann, H., Hoffmann, T., Iinuma, Y., Jang, M., Jenkin, M. E., Jimenez, J. L., Kiendler-Scharr, A., Maenhaut, W., McFiggans, G., Mentel, Th. F., Monod, A., Prévôt, A. S. H., Seinfeld, J. H., Surratt, J. D., Szmigielski, R., and Wildt, J.: The formation, properties and impact of secondary organic aerosol: current and emerging issues, *Atmos. Chem. Phys.*, 9, 5155–5236, <https://doi.org/10.5194/acp-9-5155-2009>, 2009.
- Hayes, P. L., Carlton, A. G., Baker, K. R., Ahmadov, R., Washenfelder, R. A., Alvarez, S., Rappenglück, B., Gilman, J. B., Kuster, W. C., de Gouw, J. A., Zotter, P., Prévôt, A. S. H., Szidat, S., Kleindienst, T. E., Offenberg, J. H., Ma, P. K., and Jimenez, J. L.: Modeling the formation and aging of secondary organic aerosols in Los Angeles during CalNex 2010, *Atmos. Chem. Phys.*, 15, 5773–5801, <https://doi.org/10.5194/acp-15-5773-2015>, 2015.
- Hearn, J. D. and Smith, G. D.: Kinetics and Product Studies for Ozonolysis Reactions of Organic Particles Using Aerosol CIMS, *J. Phys. Chem. A*, 108, 10019–10029, <https://doi.org/10.1021/jp0404145>, 2004.
- Hoffmann, T., Odum, J. R., Bowman, F., Collins, D., Klockow, D., Flagan, R. C., and Seinfeld, J. H.: Formation of Organic Aerosols from the Oxidation of Biogenic Hydrocarbons, *J. Atmos. Chem.*, 26, 189–222, <https://doi.org/10.1023/A:1005734301837>, 1997.
- Hu, W., Palm, B. B., Day, D. A., Campuzano-Jost, P., Krechmer, J. E., Peng, Z., de Sá, S. S., Martin, S. T., Alexander, M. L., Baumann, K., Hacker, L., Kiendler-Scharr, A., Koss, A. R., de Gouw, J. A., Goldstein, A. H., Seco, R., Sjøstedt, S. J., Park, J.-H., Guenther, A. B., Kim, S., Canonaco, F., Prévôt, A. S. H., Brune, W. H., and Jimenez, J. L.: Volatility and lifetime against OH heterogeneous reaction of ambient isoprene-epoxydiols-derived secondary organic aerosol (IEPOX-SOA), *Atmos. Chem. Phys.*, 16, 11563–11580, <https://doi.org/10.5194/acp-16-11563-2016>, 2016.
- Jathar, S. H., Cappa, C. D., Wexler, A. S., Seinfeld, J. H., and Kleeman, M. J.: Multi-generational oxidation model to simulate secondary organic aerosol in a 3-D air quality model, *Geosci. Model Dev.*, 8, 2553–2567, <https://doi.org/10.5194/gmd-8-2553-2015>, 2015.
- Kang, E., Root, M. J., Toohey, D. W., and Brune, W. H.: Introducing the concept of Potential Aerosol Mass (PAM), *Atmos. Chem. Phys.*, 7, 5727–5744, <https://doi.org/10.5194/acp-7-5727-2007>, 2007.
- Kang, E., Toohey, D. W., and Brune, W. H.: Dependence of SOA oxidation on organic aerosol mass concentration and OH exposure: experimental PAM chamber studies, *Atmos. Chem. Phys.*, 11, 1837–1852, <https://doi.org/10.5194/acp-11-1837-2011>, 2011.
- Karjalainen, P., Timonen, H., Saukko, E., Kuuluvainen, H., Saarikoski, S., Aakko-Saksa, P., Murtonen, T., Bloss, M., Dal Maso, M., Simonen, P., Ahlberg, E., Svenningsson, B., Brune, W. H., Hillamo, R., Keskinen, J., and Rönkkö, T.: Time-resolved

- characterization of primary particle emissions and secondary particle formation from a modern gasoline passenger car, *Atmos. Chem. Phys.*, 16, 8559–8570, <https://doi.org/10.5194/acp-16-8559-2016>, 2016.
- Krechmer, J. E., Pagonis, D., Ziemann, P. J., and Jimenez, J. L.: Quantification of Gas-Wall Partitioning in Teflon Environmental Chambers Using Rapid Bursts of Low-Volatility Oxidized Species Generated in Situ, *Environ. Sci. Technol.*, 50, 5757–5765, <https://doi.org/10.1021/acs.est.6b00606>, 2016.
- Lakey, P. S. J., George, I. J., Whalley, L. K., Baeza-Romero, M. T. and Heard, D. E.: Measurements of the HO₂ Uptake Coefficients onto Single Component Organic Aerosols, *Environ. Sci. Technol.*, 49, 4878–4885, <https://doi.org/10.1021/acs.est.5b00948>, 2015.
- Lambe, A., Massoli, P., Zhang, X., Canagaratna, M., Nowak, J., Daube, C., Yan, C., Nie, W., Onasch, T., Jayne, J., Kolb, C., Davidovits, P., Worsnop, D., and Brune, W.: Controlled nitric oxide production via O(¹D)+N₂O reactions for use in oxidation flow reactor studies, *Atmos. Meas. Tech.*, 10, 2283–2298, <https://doi.org/10.5194/amt-10-2283-2017>, 2017.
- Lambe, A. T. and Jimenez, J. L.: PAM Wiki: Publications Using the PAM Oxidation Flow Reactor, available at: <https://sites.google.com/site/pamwiki/publications>, last access: 27 September 2017.
- Lambe, A. T., Ahern, A. T., Williams, L. R., Slowik, J. G., Wong, J. P. S., Abbatt, J. P. D., Brune, W. H., Ng, N. L., Wright, J. P., Croasdale, D. R., Worsnop, D. R., Davidovits, P., and Onasch, T. B.: Characterization of aerosol photooxidation flow reactors: heterogeneous oxidation, secondary organic aerosol formation and cloud condensation nuclei activity measurements, *Atmos. Meas. Tech.*, 4, 445–461, <https://doi.org/10.5194/amt-4-445-2011>, 2011.
- Levy II, H.: Normal atmosphere: large radical and formaldehyde concentrations predicted, *Science*, 173, 141–143, <https://doi.org/10.1126/science.173.3992.141>, 1971.
- Li, R., Palm, B. B., Borbon, A., Graus, M., Warneke, C., Ortega, A. M., Day, D. A., Brune, W. H., Jimenez, J. L., and de Gouw, J. A.: Laboratory Studies on Secondary Organic Aerosol Formation from Crude Oil Vapors, *Environ. Sci. Technol.*, 47, 12566–12574, <https://doi.org/10.1021/es402265y>, 2013.
- Li, R., Palm, B. B., Ortega, A. M., Hu, W., Peng, Z., Day, D. A., Knote, C., Brune, W. H., de Gouw, J., and Jimenez, J. L.: Modeling the radical chemistry in an Oxidation Flow Reactor (OFR): radical formation and recycling, sensitivities, and OH exposure estimation equation, *J. Phys. Chem. A*, 119, 4418–4432, <https://doi.org/10.1021/jp509534k>, 2015.
- Link, M. F., Friedman, B., Fulgham, R., Brophy, P., Galang, A., Jathar, S. H., Veres, P., Roberts, J. M. and Farmer, D. K.: Photochemical processing of diesel fuel emissions as a large secondary source of isocyanic acid (HNCO), *Geophys. Res. Lett.*, 43, 4033–4041, <https://doi.org/10.1002/2016GL068207>, 2016.
- Lippmann, M.: Health effects of tropospheric ozone, *Environ. Sci. Technol.*, 25, 1954–1962, <https://doi.org/10.1021/es00024a001>, 1991.
- Liu, P. F., Abdelmalki, N., Hung, H.-M., Wang, Y., Brune, W. H., and Martin, S. T.: Ultraviolet and visible complex refractive indices of secondary organic material produced by photooxidation of the aromatic compounds toluene and *m*-Xylene, *Atmos. Chem. Phys.*, 15, 1435–1446, <https://doi.org/10.5194/acp-15-1435-2015>, 2015.
- Mao, J., Ren, X., Brune, W. H., Olson, J. R., Crawford, J. H., Fried, A., Huey, L. G., Cohen, R. C., Heikes, B., Singh, H. B., Blake, D. R., Sachse, G. W., Diskin, G. S., Hall, S. R., and Shetter, R. E.: Airborne measurement of OH reactivity during INTEX-B, *Atmos. Chem. Phys.*, 9, 163–173, <https://doi.org/10.5194/acp-9-163-2009>, 2009.
- Martinsson, J., Eriksson, A. C., Nielsen, I. E., Malmberg, V. B., Ahlberg, E., Andersen, C., Lindgren, R., Nyström, R., Nordin, E. Z., Brune, W. H., Svenningsson, B., Swietlicki, E., Boman, C., and Pagels, J. H.: Impacts of Combustion Conditions and Photochemical Processing on the Light Absorption of Biomass Combustion Aerosol, *Environ. Sci. Technol.*, 49, 14663–14671, <https://doi.org/10.1021/acs.est.5b03205>, 2015.
- Matsunaga, A. and Ziemann, P. J.: Gas-Wall Partitioning of Organic Compounds in a Teflon Film Chamber and Potential Effects on Reaction Product and Aerosol Yield Measurements, *Aerosol Sci. Tech.*, 44, 881–892, <https://doi.org/10.1080/02786826.2010.501044>, 2010.
- Matti Maricq, M.: Chemical characterization of particulate emissions from diesel engines: A review, *J. Aerosol Sci.*, 38, 1079–1118, <https://doi.org/10.1016/j.jaerosci.2007.08.001>, 2007.
- Moise, T. and Rudich, Y.: Reactive Uptake of Ozone by Aerosol-Associated Unsaturated Fatty Acids: Kinetics, Mechanism, and Products, *J. Phys. Chem. A*, 106, 6469–6476, <https://doi.org/10.1021/jp025597e>, 2002.
- Moise, T., Talukdar, R. K., Frost, G. J., Fox, R. W., and Rudich, Y.: Reactive uptake of NO₃ by liquid and frozen organics, *J. Geophys. Res.*, 107, 4014, <https://doi.org/10.1029/2001JD000334>, 2002.
- Nehr, S., Bohn, B., Fuchs, H., Häsel, R., Hofzumahaus, A., Li, X., Rohrer, F., Tillmann, R., and Wahner, A.: Atmospheric photochemistry of aromatic hydrocarbons: OH budgets during SAPHIR chamber experiments, *Atmos. Chem. Phys.*, 14, 6941–6952, <https://doi.org/10.5194/acp-14-6941-2014>, 2014.
- Nel, A.: Air Pollution-Related Illness: Effects of Particles, *Science*, 308, 804–806, <https://doi.org/10.1126/science.1108752>, 2005.
- Ng, N. L., Canagaratna, M. R., Zhang, Q., Jimenez, J. L., Tian, J., Ulbrich, I. M., Kroll, J. H., Docherty, K. S., Chhabra, P. S., Bahreini, R., Murphy, S. M., Seinfeld, J. H., Hildebrandt, L., Donahue, N. M., DeCarlo, P. F., Lanz, V. A., Prévôt, A. S. H., Dinar, E., Rudich, Y., Worsnop, D. R.: Organic aerosol components observed in Northern Hemispheric datasets from Aerosol Mass Spectrometry, *Atmos. Chem. Phys.*, 10, 4625–4641, <https://doi.org/10.5194/acp-10-4625-2010>, 2010.
- Odum, J. R., Hoffmann, T., Bowman, F., Collins, D., Flagan Richard, C., and Seinfeld, J. H.: Gas particle partitioning and secondary organic aerosol yields, *Environ. Sci. Technol.*, 30, 2580–2585, <https://doi.org/10.1021/es950943+>, 1996.
- Orlando, J. J. and Tyndall, G. S.: Laboratory studies of organic peroxy radical chemistry: an overview with emphasis on recent issues of atmospheric significance, *Chem. Soc. Rev.*, 41, 6294, <https://doi.org/10.1039/c2cs35166h>, 2012.
- Ortega, A. M., Day, D. A., Cubison, M. J., Brune, W. H., Bon, D., de Gouw, J. A., and Jimenez, J. L.: Secondary organic aerosol formation and primary organic aerosol oxidation from biomass-burning smoke in a flow reactor during FLAME-3, *Atmos. Chem. Phys.*, 13, 11551–11571, <https://doi.org/10.5194/acp-13-11551-2013>, 2013.

- Ortega, A. M., Hayes, P. L., Peng, Z., Palm, B. B., Hu, W., Day, D. A., Li, R., Cubison, M. J., Brune, W. H., Graus, M., Warneke, C., Gilman, J. B., Kuster, W. C., de Gouw, J., Gutiérrez-Montes, C., and Jimenez, J. L.: Real-time measurements of secondary organic aerosol formation and aging from ambient air in an oxidation flow reactor in the Los Angeles area, *Atmos. Chem. Phys.*, 16, 7411–7433, <https://doi.org/10.5194/acp-16-7411-2016>, 2016.
- Palm, B. B., Campuzano-Jost, P., Ortega, A. M., Day, D. A., Kaser, L., Jud, W., Karl, T., Hansel, A., Hunter, J. F., Cross, E. S., Kroll, J. H., Peng, Z., Brune, W. H., and Jimenez, J. L.: In situ secondary organic aerosol formation from ambient pine forest air using an oxidation flow reactor, *Atmos. Chem. Phys.*, 16, 2943–2970, <https://doi.org/10.5194/acp-16-2943-2016>, 2016.
- Palm, B. B., Campuzano-Jost, P., Day, D. A., Ortega, A. M., Fry, J. L., Brown, S. S., Zarzana, K. J., Dube, W., Wagner, N. L., Draper, D. C., Kaser, L., Jud, W., Karl, T., Hansel, A., Gutiérrez-Montes, C. and Jimenez, J. L.: Secondary organic aerosol formation from in situ OH, O₃, and NO₃ oxidation of ambient forest air in an oxidation flow reactor, *Atmos. Chem. Phys.*, 17, 5331–5354, <https://doi.org/10.5194/acp-17-5331-2017>, 2017.
- Peng, Z., Carrasco, N., and Pernot, P.: Modeling of synchrotron-based laboratory simulations of Titan's ionospheric photochemistry, *Geo. Res. J.*, 1–2, 33–53, <https://doi.org/10.1016/j.grj.2014.03.002>, 2014.
- Peng, Z., Day, D. A., Ortega, A. M., Palm, B. B., Hu, W., Stark, H., Li, R., Tsigaridis, K., Brune, W. H., and Jimenez, J. L.: Non-OH chemistry in oxidation flow reactors for the study of atmospheric chemistry systematically examined by modeling, *Atmos. Chem. Phys.*, 16, 4283–4305, <https://doi.org/10.5194/acp-16-4283-2016>, 2016.
- Peng, Z., Day, D. A., Stark, H., Li, R., Lee-Taylor, J., Palm, B. B., Brune, W. H., and Jimenez, J. L.: HO_x radical chemistry in oxidation flow reactors with low-pressure mercury lamps systematically examined by modeling, *Atmos. Meas. Tech.*, 8, 4863–4890, <https://doi.org/10.5194/amt-8-4863-2015>, 2015.
- Ranney, A. P. and Ziemann, P. J.: Kinetics of Acid-Catalyzed Dehydration of Cyclic Hemiacetals in Organic Aerosol Particles in Equilibrium with Nitric Acid Vapor, *J. Phys. Chem. A*, 120, 2561–2568, <https://doi.org/10.1021/acs.jpca.6b01402>, 2016.
- Richards-Henderson, N. K., Goldstein, A. H., and Wilson, K. R.: Large Enhancement in the Heterogeneous Oxidation Rate of Organic Aerosols by Hydroxyl Radicals in the Presence of Nitric Oxide, *J. Phys. Chem. Lett.*, 6, 4451–4455, <https://doi.org/10.1021/acs.jpclett.5b02121>, 2015.
- Saltelli, A., Ratto, M., Tarantola, S., and Campolongo, F.: Sensitivity Analysis for Chemical Models, *Chem. Rev.*, 105, 2811–2828, <https://doi.org/10.1021/cr040659d>, 2005.
- Sander, S. P., Friedl, R. R., Barker, J. R., Golden, D. M., Kurylo, M. J., Wine, P. H., Abbatt, J. P. D., Burkholder, J. B., Kolb, C. E., Moortgat, G. K., Huie, R. E., and Orkin, V. L.: Chemical Kinetics and Photochemical Data for Use in Atmospheric Studies, Evaluation Number 7, Pasadena, CA, USA, available at: <http://jpldataeval.jpl.nasa.gov/pdf/JPL10-6Final> (last access: June 2016), 2011.
- Schill, G. P., Jathar, S. H., Kodros, J. K., Levin, E. J. T., Galang, A. M., Friedman, B., Link, M. F., Farmer, D. K., Pierce, J. R., Kreidenweis, S. M., and DeMott, P. J.: Ice-nucleating particle emissions from photochemically aged diesel and biodiesel exhaust, *Geophys. Res. Lett.*, 43, 5524–5531, <https://doi.org/10.1002/2016GL069529>, 2016.
- Schwantes, R. H., Schilling, K. A., McVay, R. C., Lignell, H., Coggon, M. M., Zhang, X., Wennberg, P. O., and Seinfeld, J. H.: Formation of highly oxygenated low-volatility products from cresol oxidation, *Atmos. Chem. Phys.*, 17, 3453–3474, <https://doi.org/10.5194/acp-17-3453-2017>, 2017.
- Seakins, P. W.: A brief review of the use of environmental chambers for gas phase studies of kinetics, chemical mechanisms and characterisation of field instruments, *EPJ Web Conf.*, 9, 143–163, <https://doi.org/10.1051/epjconf/201009012>, 2010.
- Simonen, P., Saukko, E., Karjalainen, P., Timonen, H., Bloss, M., Aakko-Saksa, P., Rönkkö, T., Keskinen, J., and Dal Maso, M.: A new oxidation flow reactor for measuring secondary aerosol formation of rapidly changing emission sources, *Atmos. Meas. Tech.*, 10, 1519–1537, <https://doi.org/10.5194/amt-10-1519-2017>, 2017.
- Stocker, T. F., Qin, D., Plattner, G.-K., Tignor, M., Allen, S. K., Boschung, J., Nauels, A., Xia, Y., Bex, V., and Midgley, P. M.: *Climate Change 2013 – The Physical Science Basis*, edited by: Intergovernmental Panel on Climate Change, Cambridge University Press, Cambridge, 2014.
- Strollo, C. M. and Ziemann, P. J.: Products and mechanism of secondary organic aerosol formation from the reaction of 3-methylfuran with OH radicals in the presence of NO_x, *Atmos. Environ.*, 77, 534–543, <https://doi.org/10.1016/j.atmosenv.2013.05.033>, 2013.
- Tkacik, D. S., Lambe, A. T., Jathar, S., Li, X., Presto, A. A., Zhao, Y., Blake, D., Meinardi, S., Jayne, J. T., Croteau, P. L., and Robinson, A. L.: Secondary Organic Aerosol Formation from in-Use Motor Vehicle Emissions Using a Potential Aerosol Mass Reactor, *Environ. Sci. Technol.*, 48, 11235–11242, <https://doi.org/10.1021/es502239v>, 2014.
- Volkamer, R., Jimenez, J. L., San Martini, F., Dzepina, K., Zhang, Q., Salcedo, D., Molina, L. T., Worsnop, D. R., and Molina, M. J.: Secondary organic aerosol formation from anthropogenic air pollution: Rapid and higher than expected, *Geophys. Res. Lett.*, 33, L17811, <https://doi.org/10.1029/2006GL026899>, 2006.
- Wang, J., Doussin, J. F., Perrier, S., Perraudin, E., Katrib, Y., Pangu, E., and Picquet-Varrault, B.: Design of a new multi-phase experimental simulation chamber for atmospheric photochemical aerosol and cloud chemistry research, *Atmos. Meas. Tech.*, 4, 2465–2494, <https://doi.org/10.5194/amt-4-2465-2011>, 2011.
- Zhang, X., Cappa, C. D., Jathar, S. H., McVay, R. C., Ensberg, J. J., Kleeman, M. J., and Seinfeld, J. H.: Influence of vapor wall loss in laboratory chambers on yields of secondary organic aerosol, *P. Natl. Acad. Sci. USA*, 111, 5802–5807, <https://doi.org/10.1073/pnas.1404727111>, 2014.
- Ziemann, P. J. and Atkinson, R.: Kinetics, products, and mechanisms of secondary organic aerosol formation, *Chem. Soc. Rev.*, 41, 6582, <https://doi.org/10.1039/c2cs35122f>, 2012.